Mechanics of Materials 95 (2016) 204–222

Contents lists available at ScienceDirect

Mechanics of Materials

journal homepage: www.elsevier.com/locate/mechmat

Effective in-plane elastic properties of auxetic honeycombs with spatial irregularity

T. Mukhopadhyay*, S. Adhikari

College of Engineering, Swansea University, Swansea, UK

ARTICLE INFO

Article history:
Received 22 August 2015
Revised 15 December 2015
Available online 2 February 2016

Keywords:
Auxetic honeycomb
Irregularity
Negative Poisson's ratio
Elastic moduli
Cellular structure
Random cell angle

ABSTRACT

An analytical framework has been developed for predicting the equivalent in-plane elastic moduli (longitudinal and transverse Young's modulus, shear modulus, Poisson's ratios) of irregular auxetic honeycombs with spatially random variations in cell angles. Employing a bottom up multi-scale based approach, computationally efficient closed-form expressions have been derived in this article. This study also includes development of a highly generalized finite element code capable of accepting number of cells in two perpendicular directions, random structural geometry and material properties of irregular auxetic honeycomb and thereby obtaining five in-plane elastic moduli of the structure. The elastic moduli obtained for different degree of randomness following the analytical formulae have been compared with the results of direct finite element simulations and they are found to be in good agreement corroborating the validity and accuracy of the proposed approach. The transverse Young's modulus, shear modulus and Poisson's ratio for loading in transverse direction (effecting the auxetic property) have been found to be highly influenced by the structural irregularity in auxetic honeycombs.

1. Introduction

The materials having negative Poisson's ratio are called auxetic material, which exhibits an unusual yet fascinating property of being thicker in dimension perpendicular to the direction of stretching and vice-versa (Evans and Alderson, 2000; Evans et al., 1991). The auxetic behavior in global response of these materials is developed by some specific arrangement of the micro-structural geometry, which allows the material to deform in a particular manner that results the negative Poisson's ratio (refer Fig. 1, for demonstration of auxetic and non-auxetic behaviour of hexagonal honeycombs). This class of materials have attracted considerable attention in last few decades due to their unusual characteristics leading to several application specific desirable engineering properties such as high indentation resistance, increased shear stiffness, increased plane strain fracture toughness, enhanced resistance to buckling under pure bending, superior permeability, enhanced acoustic absorption capacity and direct structural properties like formation of double curvature under flexure (Yang et al., 2004; Evans and Alderson, 2000; Overaker et al., 1998; Stavroulakis, 2005; Critchley et al., 2013; Yao et al., 2008; Bacigalupo and Bellis, 2015; Bacigalupo and Gambarotta, 2014; Scarpa et al., 2003; Yang et al., 2015; Grima et al., 2015; Rad et al., 2014; Nkansah et al., 1994). Moreover natural as well as man made auxetic materials and structural forms can be found across different length-scales strating from nano to macro scale (Evans and Alderson, 2000), wherein the underlying theory of elasticity for analysing mechanical properties of these materials remain same. Thus study of the mechanics behind different forms of such materials have always been of

* Corresponding author.
E-mail addresses: 800712@swansea.ac.uk, mukhopadhyay.mail@gmail.com (T. Mukhopadhyay), S.Adhikari@swansea.ac.uk (S. Adhikari).
URL: http://www.tmukhopadhyay.com (T. Mukhopadhyay)

http://dx.doi.org/10.1016/j.mechmat.2016.01.009
0167-6636/

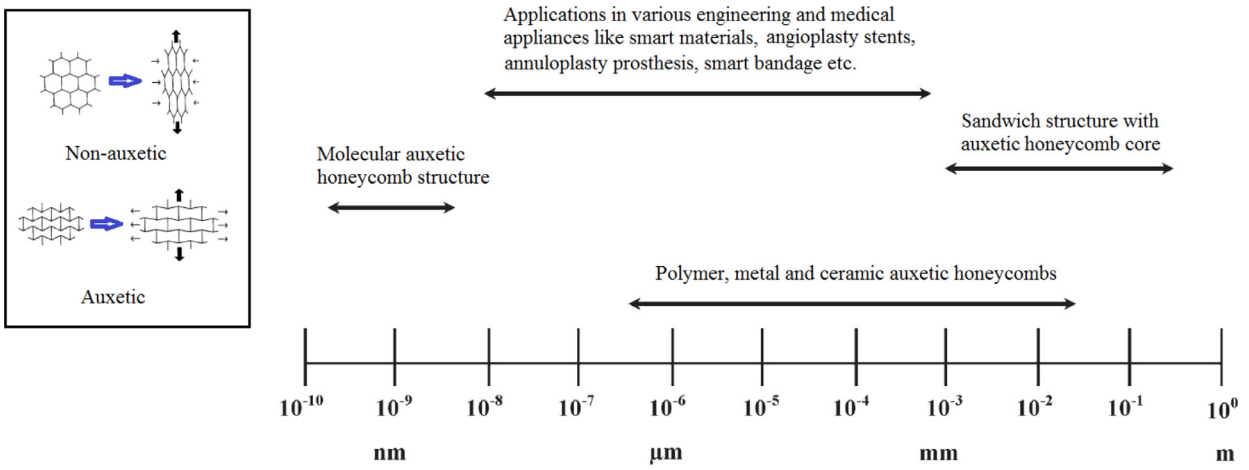

Fig. 1. Occurrence and application of auxetic hexagonal honeycombs across the length scales.

profound interest to the research community since the discovery of auxetic materials. For details about different forms of auxetic materials readers can refer to (Evans and Alderson, 2000). The present article concentrates on auxetic re-entrant hexagonal honeycombs, a brief review of which is presented in the next paragraph.

In last couple of decades, application of hexagonal auxetic lattice forms have been explored from atomic scale to macro scale, in a vast domain ranging from engineering to bio-medical technology. Fig. 1 shows the presence of auxetic re-entrant honeycombs of hexagonal structural form in different length scales. Some of the previous articles (Evans and Alderson, 2000; Nkansah et al., 1994; Karnessis and Burriesci, 2013; Wang and Hu, 2014; Sun et al., 2014; Scarpa and Tomlinson, 2000) have discussed this considering different forms of auxetic materials, in general. Fig. 1 emphasizes on the occurance and application of hexagonal auxetic honeycombs only, according to the aim and scope of the present work. Auxetic character in such hexagonal lattices develops due to the re-entrant shape of their unit cell, as easily perceivable from the figure. The closed form formulae for regular honeycombs provided by Gibson and Ashby (1999) are widely used to obtain in-plane elastic moduli of auxetic honeycombs. Recently new analytical formulae for regular hexagonal honeycombs have been reported considering the nodes at the intersections of inclined and vertical members by Malek and Gibson (2015). Effect of hierarchy in lattices have also been studied by many researchers (Banerjee, 2014). Gereke et al. (2012) have presented a multi-scale stochastic modelling approach for elastic properties of strand-based wood composites. Several studies can be found in available literature dealing with mechanical properties of regular auxetic honeycombs using numerical and experimental investigations (Scarpa et al., 2000; Scarpa and Tomlin, 2000; Grima et al., 2013; Scarpa et al., 2003). Available analytical approaches for obtaining equivalent elastic moduli of auxetic honeycombs are based on unit cell approach, which fails to account for any form of irregularity in the structure. Spatial irregularity in auxetic honeycomb may occur due to uncertainty associated with manufacturing in macro-level and process of fabrication and synthesizing in molecular level, uncertain distribution of intrinsic material properties, structural defects, variation in temperature, pre-stressing and micro-structural variability. Several investigations to explore the effect of irregularity are found to have concentrated on non-auxetic honeycombs including voronoi honeycombs (Li et al., 2007; Triantafyllidis and Schraad, 1998; Ajdari et al., 2008; Zhu et al., 2001; Li et al., 2005; Alsayednoor et al., 2013; Mukhopadhyay and Adhikari, 2016). Papka and Kyriakides (1994) have carried out numerical and experimental study of honeycomb crushing behaviour considering geometrical imperfections in the structure such as variation in length of bond line and over or under expanded cells. The state of available literature which investigates the effect of irregularity in auxetic honeycombs is very scarce. Recently (Liu et al., 2014) have investigated manufacturing irregularity in auxetic honeycomb using finite element analysis. They have reported that structural irregularity influences the effective elastic modulus, yield strength and Poisson's ratio of auxetic honeycombs. All the studies mentioned above exploring the effect of irregularity in both auxetic as well as non-auxetic honecombs are based on either finite element simulations or experimental investigations. Experimental investigations are very expensive and time consuming, which makes it practically not feasible to capture the effect of random irregularities in honeycomb structure in a robust and comprehensive manner by testing huge number of samples. The finite element approach becomes quite computationally intensive because a small change in geometry of a single cell may require creating completely new geometry and meshing the entire structure. Moreover when irregular honeycombs are modelled as a part of another host structure, the degree of freedom to be considered becomes very high making it prohibitively expensive to simulate. The problem becomes even worse for uncertainty quantification using a Monte Carlo based approach (Hurtado and Barbat, 1998; Dey et al., 2015a; 2015b), where the expensive finite element model is needed to be simulated for a large number of samples with different structural configurations. A simple yet computationally efficient way to

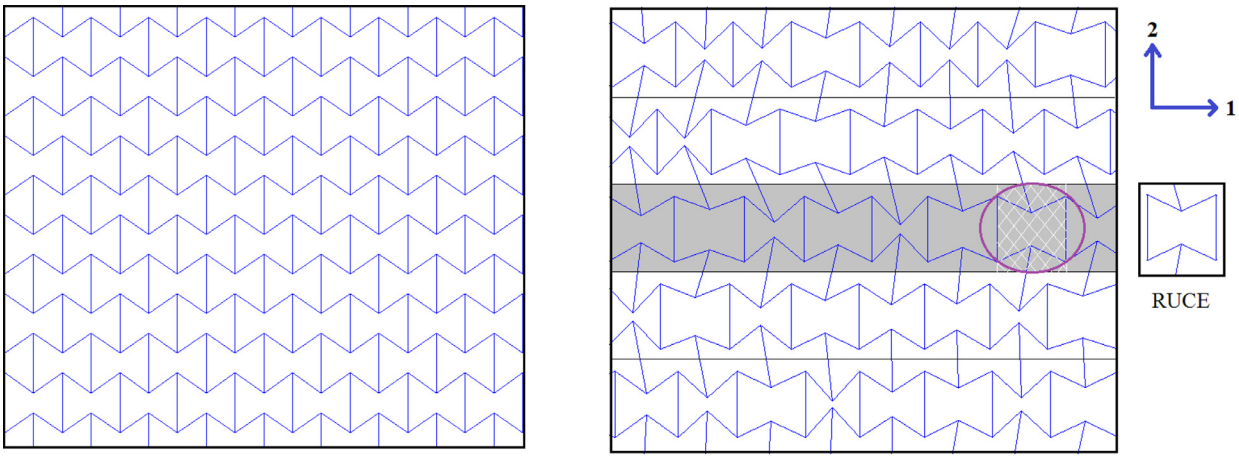

Fig. 2. Typical representation of regular and irregular auxetic honeycomb structure.

characterize the elastic properties of irregular auxetic honeycomb could be following an analytical approach.

This article develops an analytical framework leading to closed form formulae for predicting equivalent in-plane elastic properties of irregular auxetic honeycomb having spatially random variations in cell angle. Subsequently the effect of irregularity on the auxetic properties of such honeycombs are discussed. To the best of authors' knowledge, no such closed form formulae for irregular auxetic honeycomb are available in literature. This article is organized as follows hereafter, Section 2: derivations of closed form formulae for five in-plane elastic moduli of irregular auxetic honeycombs; Section 3: development of finite element model to obtain the in-plane elastic moduli of irregular auxetic honeycomb numerically for validating the proposed analytical approach; Section 4: results and discussion based on both the proposed analytical approach and the finite element code. A comparative inference has been drawn in this section establishing validity of the developed analytical expressions; and Section 5: concise summary and conclusion.

2. Elastic properties of irregular auxetic honeycombs

A bottom up approach has been proposed in this article for deriving expressions of effective in-plane elastic moduli for irregular auxetic honeycombs. The key philosophy behind the proposed idea is that the entire irregular auxetic honeycomb structure is considered to be consisted of several representative unit cell elements (as shown in Fig. 2(b)) having different individual elastic moduli depending on its structural geometry and material properties. In the elementary local level, effect of irregularity is accounted by analysing the representative unit cell elements (RUCEs) first and then this effect of irregularity is propagated towards the global properties of the entire structure in a multi-scale framework through a multi-stage process as shown in Fig. 6. The expressions for elastic moduli of a single RUCE are derived first (as discussed in Section 2.1) and subsequently the expressions for effective in-plane elastic moduli of the entire irregular auxetic honeycomb are derived using basic principles of mechanics (as discussed in Section 2.2). The entire process of deriving expressions for each of the elastic modulus of the entire irregular auxetic honeycomb consists of four stages: selection of appropriate RUCE and proper idealization scheme; derivation of the expressions for elastic moduli of a single RUCE; derivation of equivalent elastic moduli for each strip and finally, derivation of elastic moduli of the entire irregular auxetic honeycomb. The RUCEs have been chosen from the viewpoint of the adopted discretization scheme (Fig. 6) in the proposed bottom-up approach. One of the most important criteria is that the chosen form of RUCE should reasonably allow us to assemble their individual properties in the 'strip' level first, and thereby in the 'global' level considering idealized blocks. Here the RUCEs are basically the representative building blocks of the entire irregular honeycomb. Elastic properties (Z_U) of the RUCEs can be represented as a function of structural irregularity $Z_U(\omega)$, where the parameter ω captures the random structural geometry/ irregularity of a particular RUCE. Here Z and U denote a particular elastic modulus and representative unit (RUCE), respectively. It is worthy to mention here that effectively three loading directions are needed to be considered for deriving the expressions of five in-plane elastic moduli as shown in Fig. 6. For longitudinal Young's modulus (E_1) and Poisson's ratio ν_{12}, stress σ_1 is applied in direction-1 (Fig. 2(b)), while for transverse Young's modulus (E_2) and Poisson's ratio ν_{21}, stress σ_2 is applied in direction-2. To obtain the expression of shear modulus (G_{12}), shear stress τ is applied as shown in Fig. 6. The notations used for different elastic moduli throughout this article are as follows: Z_U denotes elastic moduli of a single RUCE; $\hat{Z}$ denotes equivalent elastic moduli of a single strip; Z_{eq} denotes equivalent elastic moduli of the entire irregular auxetic honeycomb, where Z is a particular elastic modulus under consideration. The subscripts i and j have been used to indicate position of the RUCE or a single

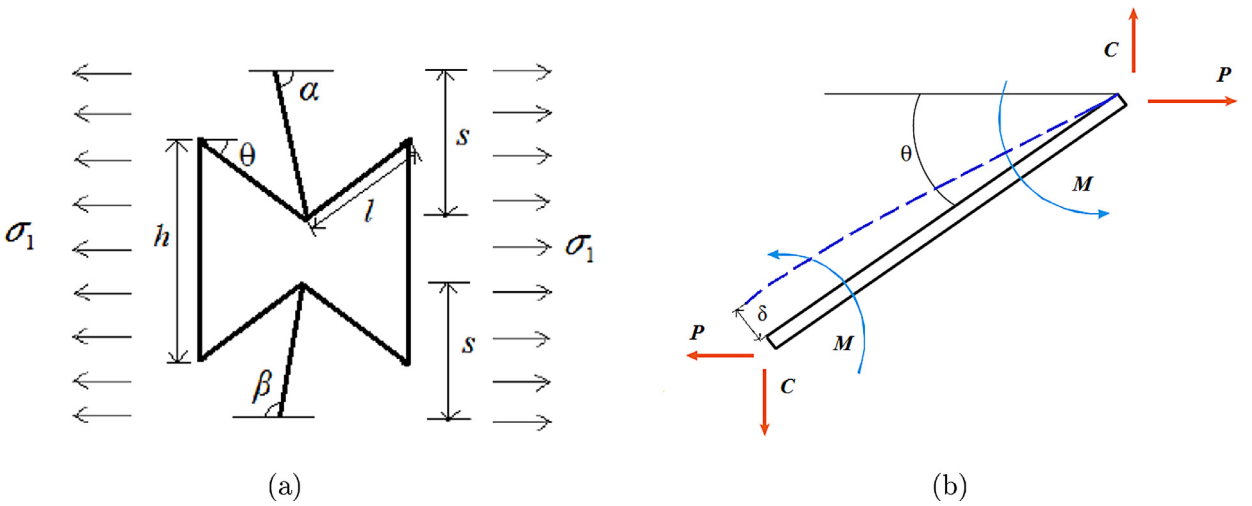

Fig. 3. RUCE and free-body diagram used in the proposed analysis for E_{1U}.

strip under consideration. The formulae proposed here are applicable for both tensile as well as compressive stresses.

2.1. Derivation of expressions for elastic moduli of a single RUCE

Derivation of expressions for the five different in-plane elastic moduli of a single RUCE is discussed in this section. These expressions will be utilized to obtain final closed form formulae of the entire irregular auxetic honeycomb in subsequent sections.

2.1.1. Longitudinal Young's modulus (E_{1U})

To derive the expression of longitudinal Young's modulus for a RUCE (E_{1U}), stress σ_1 is applied in direction-1 (refer Fig. 2, for direction) as shown in Fig. 3. The inclined cell walls having inclination angle α and β do not have any contribution in the analysis of E_{1U}, as the stresses applied on them in two opposite directions neutralise each other. It can be noticed that the remaining structure except these two inclined cell walls is symmetric. The applied stresses cause the inclined cell walls having inclination angle θ to bend and this contributes to the overall deformation of the structure in direction-1. From the condition of equilibrium, the vertical forces C in the free-body diagram of these cell walls (refer Fig. 3) need to be zero. In the present analysis the cell walls are treated as beams of thickness t, depth b and Young's modulus E_s. l and h are the lengths of inclined cell walls having inclination angle θ and the vertical cell walls respectively as shown in Fig. 3(a). From Fig. 3(b) (similar to Gibson and Ashby, 1999; Wan et al., 2004),

$$M = \frac{Pl\sin\theta}{2} \tag{1}$$

where

$$P = \sigma_1(h - l\sin\theta)b \tag{2}$$

From the standard beam theory (Roark and Young, 1976), the deflection of one end compared to the other end of the cell wall shown in Fig. 3(b) can be expressed as

$$\delta = \frac{Pl^3\sin\theta}{12E_sI} \tag{3}$$

where I is the second moment of inertia of the cell wall, that is $I = bt^3/12$.

The component of δ parallel to direction-1 is $\delta\sin\theta$. The strain parallel to direction-1 becomes

$$\epsilon_1 = \frac{\delta\sin\theta}{l\cos\theta} \tag{4}$$

Thus the Young's modulus in direction-1 for a RUCE can be expressed as

$$E_{1U} = \frac{\sigma_1}{\epsilon_1} = E_s\left(\frac{t}{l}\right)^3\frac{\cos\theta}{(\frac{h}{l} - \sin\theta)\sin^2\theta} \tag{5}$$

2.1.2. Transverse Young's modulus (E_{2U})

To derive the expression of transverse Young's modulus for a RUCE (E_{2U}), stress σ_2 is applied in direction-2 (refer Fig. 2, for direction) as shown in Fig. 4(a). Total deformation of the RUCE in direction-2 consists of three components, namely deformation of the cell wall having inclination angle α, deformation of the cell walls having inclination angle θ and deformation of the cell wall having inclination angle β. All the cell walls are considered axially rigid in this analysis. Here in Fig. 4(a), if the remaining structure except the two inclined cell walls having inclination angle α and β is considered, two forces that act at joint B are: a vertical force (W) and a moment (M_1). Effect of the bending moment M_1 to the cell wall having inclination angle α is only to create rotation (ϕ) as shown in Fig. 4(b).

Vertical deformation of the cell wall having inclination angle α has two components, bending deformation in direction-2 and rotational deformation due the rotation of joint B as shown in Fig. 4(b). The bending deformation in direction-2 can be expressed as

$$\delta_{2vb} = \left(\frac{W\cos\alpha(\frac{s}{\sin\alpha})^3}{3E_sI}\right)\cos\alpha \tag{6}$$

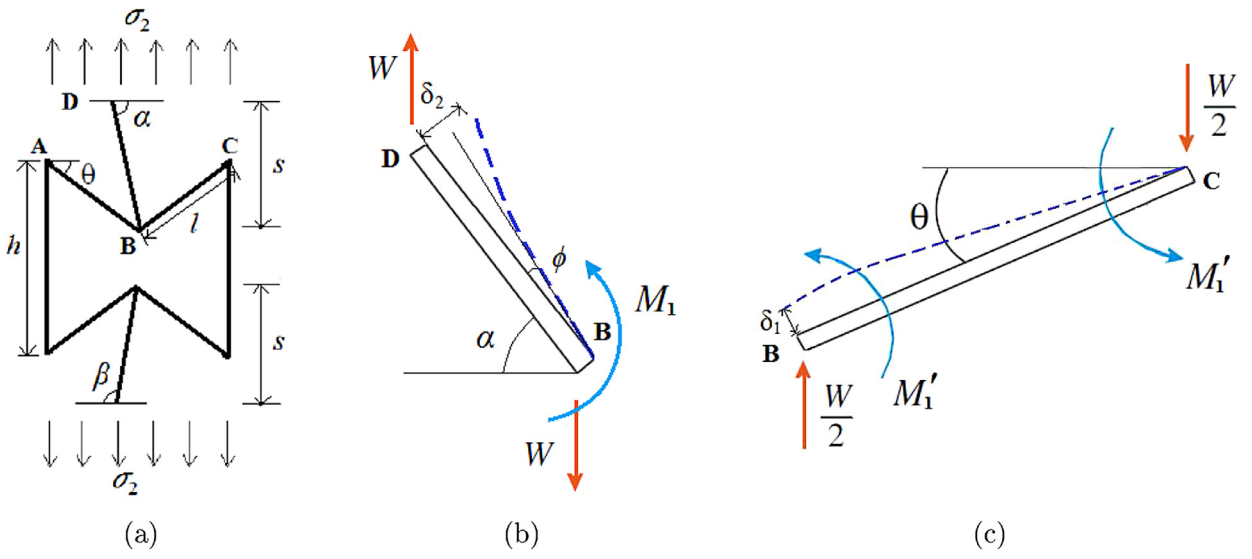

Fig. 4. RUCE and free-body diagram used in the proposed analysis for E_{2U}.

where $W = 2\sigma_2 lb\cos\theta$ and $I = bt^3/12$. From Fig. 4(b), $M_1 = Wscot\alpha$. Cell walls BC and BA will share half of moment M_1 each as they have equal stiffness. Using the standard result of Euler–Bernoulli beam theory, deflection at one end due to application of moment at the other end ($\delta = Ml^2/6E_sI$), the angle of rotation at joint B can be expressed as

$$\phi = \frac{M_1}{2}\frac{l}{6E_sI} \tag{7}$$

The component of rotational deformation of the cell wall having inclination angle α in direction-2 can be expressed as

$$\delta_{2vr} = \phi\left(\frac{s}{sin\alpha}\right)cos\alpha \tag{8}$$

Thus from Eqs. (6)–(8) after replacing $W = 2\sigma_2 lb\cos\theta$, $M_1 = Wscot\alpha$ and $I = bt^3/12$, total deformation in direction-2 of the cell wall having inclination angle α can be expressed as

$$\delta_{v2} = \delta_{2vb} + \delta_{2vr} = \frac{2\sigma_2 s^2 l\cos\theta}{E_S t^3}\left(4s\frac{\cos^2\alpha}{\sin^3\alpha} + lcot^2\alpha\right) \tag{9}$$

Deformation of the cell wall having inclination angle β in direction-2 can also be expressed in the similar way as

$$\dot{\delta}_{v2} = \frac{2\sigma_2 s^2 l\cos\theta}{E_S t^3}\left(4s\frac{\cos^2\beta}{\sin^3\beta} + lcot^2\beta\right) \tag{10}$$

From Fig. 4(c), deformation of each of the cell walls having inclination angle θ in direction-2

$$\bar{\delta}_{v1} = \frac{(\frac{W}{2}\cos\theta)l^3}{12E_sI}\cos\theta \tag{11}$$

Replacing $W = 2\sigma_2 lb\cos\theta$ and $I = bt^3/12$ from Eq. (11), total deformation in direction-2 of two cell walls having inclination angle θ can be expressed as

$$\delta_{v1} = \frac{2\sigma_2 l^4\cos^3\theta}{12E_s t^3} \tag{12}$$

Thus total deformation in direction-2 of the RUCE represented in Fig. 4(a) due to application of stresses σ_2 is

$$\begin{aligned}\delta_v &= \delta_{v2} + \dot{\delta}_{v2} + \delta_{v1}\\ &= \frac{\sigma_2 l\cos\theta}{E_s t^3}\left(2l^3\cos^2\theta + 8s^3\left(\frac{\cos^2\alpha}{\sin^3\alpha} + \frac{\cos^2\beta}{\sin^3\beta}\right)\right.\\ &\quad \left. + 2s^2 l(cot^2\alpha + cot^2\beta)\right)\end{aligned} \tag{13}$$

Strain in direction-2 can be obtained as

$$\epsilon_2 = \frac{\delta_v}{h + 2s - 2l\sin\theta} \tag{14}$$

Thus Young's modulus in direction-2 of a RUCE can be expressed as

$$\begin{aligned}E_{2U} &= \frac{\sigma_2}{\epsilon_2}\\ &= E_s\left(\frac{t}{l}\right)^3\\ &\quad \frac{(\frac{h}{l} + 2\frac{s}{l} - 2\sin\theta)}{\cos\theta(2\cos^2\theta + 8(\frac{s}{l})^3\left(\frac{\cos^2\alpha}{\sin^3\alpha} + \frac{\cos^2\beta}{\sin^3\beta}\right) + 2(\frac{s}{l})^2(cot^2\alpha + cot^2\beta))}\end{aligned} \tag{15}$$

2.1.3. Poisson's ratio ν_{12U}

Poisson's ratios are calculated by taking the negative ratio of strains normal to, and parallel to, the loading direction. Poisson's ratio of a RUCE for the loading direction-1 (ν_{12U}) is obtained as (refer Fig. 3(a))

$$\nu_{12U} = -\frac{\epsilon_2}{\epsilon_1} \tag{16}$$

where ϵ_1 and ϵ_2 represent the strains of a RUCE in direction-1 and direction-2 respectively due to loading in direction-1. ϵ_1 can be obtained from Eq. (4). From Fig. 3(b), ϵ_2 can be expressed as

$$\epsilon_2 = \frac{2\delta\cos\theta}{h - 2l\sin\theta + 2s} \tag{17}$$

Thus the expression for Poisson's ratio of a RUCE for the loading direction-1 becomes

$$\nu_{12U} = -\frac{2\cos^2\theta}{(\frac{h}{l} + 2\frac{s}{l} - 2\sin\theta)\sin\theta} \tag{18}$$

2.1.4. Poisson's ratio ν_{21U}

Poisson's ratio of a RUCE for the loading direction-2 (ν_{21U}) is obtained as (refer Fig. 4(a))

$$\nu_{21U} = -\frac{\epsilon_1}{\epsilon_2} \tag{19}$$

where ϵ_1 and ϵ_2 represent the strains of a RUCE in direction-1 and direction-2 respectively due to loading in direction-2. ϵ_2 can be obtained from Eqs. (13) and (14) as

$$\epsilon_2 = \frac{\sigma_2 l\cos\theta}{E_s t^3(h + 2s - 2l\sin\theta)} \times \left(2l^3\cos^2\theta + 8s^3\left(\frac{\cos^2\alpha}{\sin^3\alpha} + \frac{\cos^2\beta}{\sin^3\beta}\right) + 2s^2 l(cot^2\alpha + cot^2\beta)\right) \tag{20}$$

From Fig. 4(c)

$$\epsilon_1 = \frac{\delta_1\sin\theta}{l\cos\theta} \tag{21}$$

where $\delta_1 = \frac{(\frac{W}{2}\cos\theta)l^3}{12E_s I}$ and $W = 2\sigma_2 lb\cos\theta$. Thus Eq. (21) reduces to

$$\epsilon_1 = \frac{\sigma_2 l^3\sin\theta\cos\theta}{E_s t^3} \tag{22}$$

Thus the expression for Poisson's ratio of a RUCE for the loading direction-2 becomes

$$\nu_{21U} = -\frac{\sin\theta(\frac{h}{l} + 2\frac{s}{l} - 2\sin\theta)}{2\cos^2\theta + 8(\frac{s}{l})^3(\frac{\cos^2\alpha}{\sin^3\alpha} + \frac{\cos^2\beta}{\sin^3\beta}) + 2(\frac{s}{l})^2(\cot^2\alpha + \cot^2\beta)} \tag{23}$$

2.1.5. Shear modulus (G_{12U})

To derive the expression of shear modulus (G_{12U}) for a RUCE, shear stress τ is applied as shown in Fig. 5(a). Lateral deformation of point D with respect to point H consists of three components, namely lateral deformation of the cell wall having inclination angle α, lateral deformation of the vertical cell walls and lateral deformation of the cell wall having inclination angle β. The remaining structure except the two inclined cell walls having inclination angles α and β is symmetric. Thus points A, B, C (and points E, G, F) do not have any relative lateral movement under the applied stresses. For this reason, the cell walls having inclination angle θ do not have any contribution in the lateral deformation of the RUCE. From Fig. 5(b) $M = Fs$, where $F = 2\tau lb\cos\theta$. Due to equal bending stiffness of cell walls AB and BC, they will share half of moment M each. Using the standard result of Euler-Bernoulli beam theory, (deflection at one end due to application of moment at the other end $\delta = Ml^2/6E_s I$), the angle of rotation at joint B can be expressed as

$$\phi = \frac{M}{2}\frac{l}{6E_s I} = \frac{Fsl}{12E_s I} \tag{24}$$

Lateral deformation of the cell wall having inclination angle α has two components, bending deformation and rotational deformation due the rotation of joint B as shown in Fig. 5(b).

Thus the total lateral deformation of point D with respect to point B is

$$\delta_{L1} = \left(\frac{Fsin\alpha}{3EI}\left(\frac{s}{sin\alpha}\right)^3 + \phi\frac{s}{sin\alpha}\right)sin\alpha = \frac{Fs^2}{12EI}\left(l + \frac{4s}{sin\alpha}\right) \tag{25}$$

Lateral deformation the cell wall having inclination angle β can also be expressed in the similar way as

$$\delta_{L2} = \frac{Fs^2}{12EI}\left(l + \frac{4s}{sin\beta}\right) \tag{26}$$

In Fig. 5(c), J is the midpoint of the member AE. Displacement of point J with respect to point A is calculated in the similar way as above considering the rotation of point A and bending deformation of member AJ,

$$\delta_{L3} = \frac{Fh^2}{48EI}(l + 2h) \tag{27}$$

Displacement of point J in direction-1 with respect to point E (δ_{L4}) is same as δ_{L3}.

By replacing $F = 2\tau lb\cos\theta$ and $I = bt^3/12$ in Eqs. (25)–(27) total lateral movement of point D with respect to point H

$$\delta_L = \delta_{L1} + \delta_{L2} + \delta_{L3} + \delta_{L4} = \frac{2\tau l\cos\theta}{Et^3}\left(2ls^2 + h^3 + \frac{h^2 l}{2} + 4s^3\left(\frac{1}{sin\alpha} + \frac{1}{sin\beta}\right)\right) \tag{28}$$

The shear strain γ for a RUCE can be expressed as

$$\gamma = \frac{\delta_L}{2s + h - 2l\sin\theta} = \frac{2\tau l\cos\theta}{Et^3(2s + h - 2l\sin\theta)} \times \left(2ls^2 + h^3 + \frac{h^2 l}{2} + 4s^3\left(\frac{1}{sin\alpha} + \frac{1}{sin\beta}\right)\right) \tag{29}$$

Thus the expression for shear modulus of a RUCE becomes

$$G_{12U} = \frac{\tau}{\gamma} = E_s\left(\frac{t}{l}\right)^3 \frac{(2\frac{s}{l} + \frac{h}{l} - 2\sin\theta)}{2\cos\theta(2(\frac{s}{l})^2 + 4(\frac{s}{l})^3(\frac{1}{sin\alpha} + \frac{1}{sin\beta}) + (\frac{h}{l})^3 + \frac{1}{2}(\frac{h}{l})^2)} \tag{30}$$

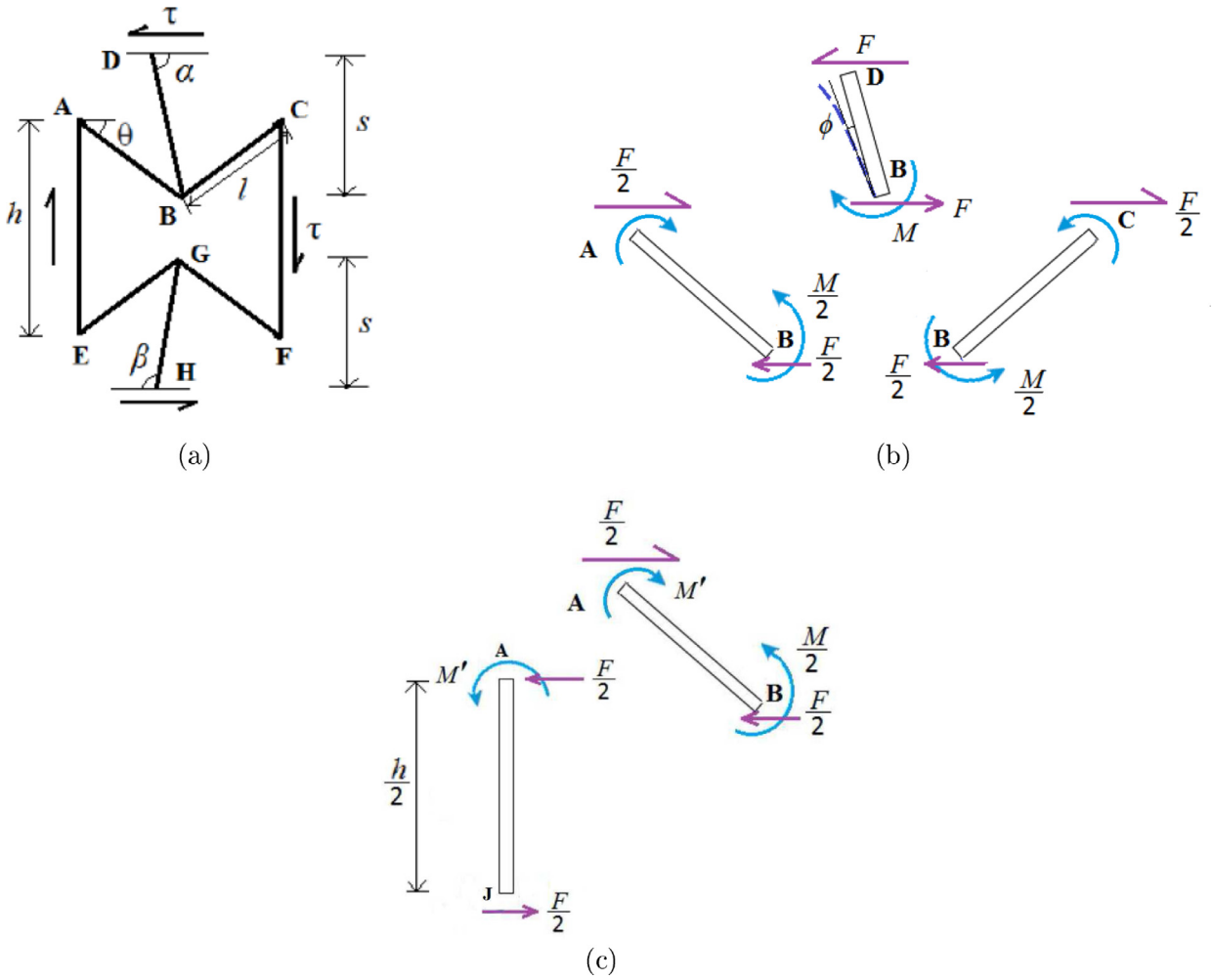

Fig. 5. RUCE and free-body diagram used in the proposed analysis for G_{12U}.

2.2. Derivation of expressions for elastic moduli of the entire irregular auxetic honeycomb structure

Derivation of closed form expressions for elastic moduli of the entire irregular auxetic honeycomb structure is discussed in this section. For this purpose the formulae for a single RUCE (Section 2.1) have been utilized and thereby a multi-step bottom up approach is followed to derive equivalent elastic moduli for a single strip and finally equivalent elastic moduli for the entire auxetic honeycomb with structural irregularity (refer Fig. 6). In the present analysis, the entire irregular honeycomb structure (Fig. 2(b)) is assumed to have m and n number of RUCEs in direction-1 and direction-2, respectively. A particular cell having position at ith column and jth row is represented as (i, j), where $i = 1, 2, \ldots, m$ and $j = 1, 2, \ldots, n$.

2.2.1. Longitudinal Young's modulus (E_{1eq})

To obtain E_{1eq}, stress σ_1 is applied in direction-1 as shown in Fig. 6. Fig. 6 consists of three groups of loading directions considered in this study. For the analysis of E_{1eq}, we need to consider the group with loading in direction-1. If the deformation compatibility condition of jth strip is considered, the total deformation due to stress σ_1 of that particular strip (Δ_1) is the summation of individual deformations of each RUCEs in direction-1, while deformation of each of these RUCEs in direction-2 are same. Thus for the jth strip

$$\Delta_1 = \sum_{i=1}^{m} \Delta_{1ij} \tag{31}$$

The Eq. (31) can be rewritten as

$$\epsilon_1 L = \sum_{i=1}^{m} \epsilon_{1ij} L_{ij} \tag{32}$$

where ϵ_1 and L represent strain and dimension in direction-1 of respective elements. Eq. (32) leads to

$$\frac{\sigma_1 L}{\hat{E_{1j}}} = \sum_{i=1}^{m} \frac{\sigma_1 L_{ij}}{E_{1Uij}} \tag{33}$$

From Eq. (33), equivalent Young's modulus of jth strip ($\hat{E_{1j}}$) can be expressed as

$$\hat{E_{1j}} = \frac{\sum_{i=1}^{m} l_{ij} \cos\theta_{ij}}{\sum_{i=1}^{m} \frac{l_{ij}\cos\theta_{ij}}{E_{1Uij}}} \tag{34}$$

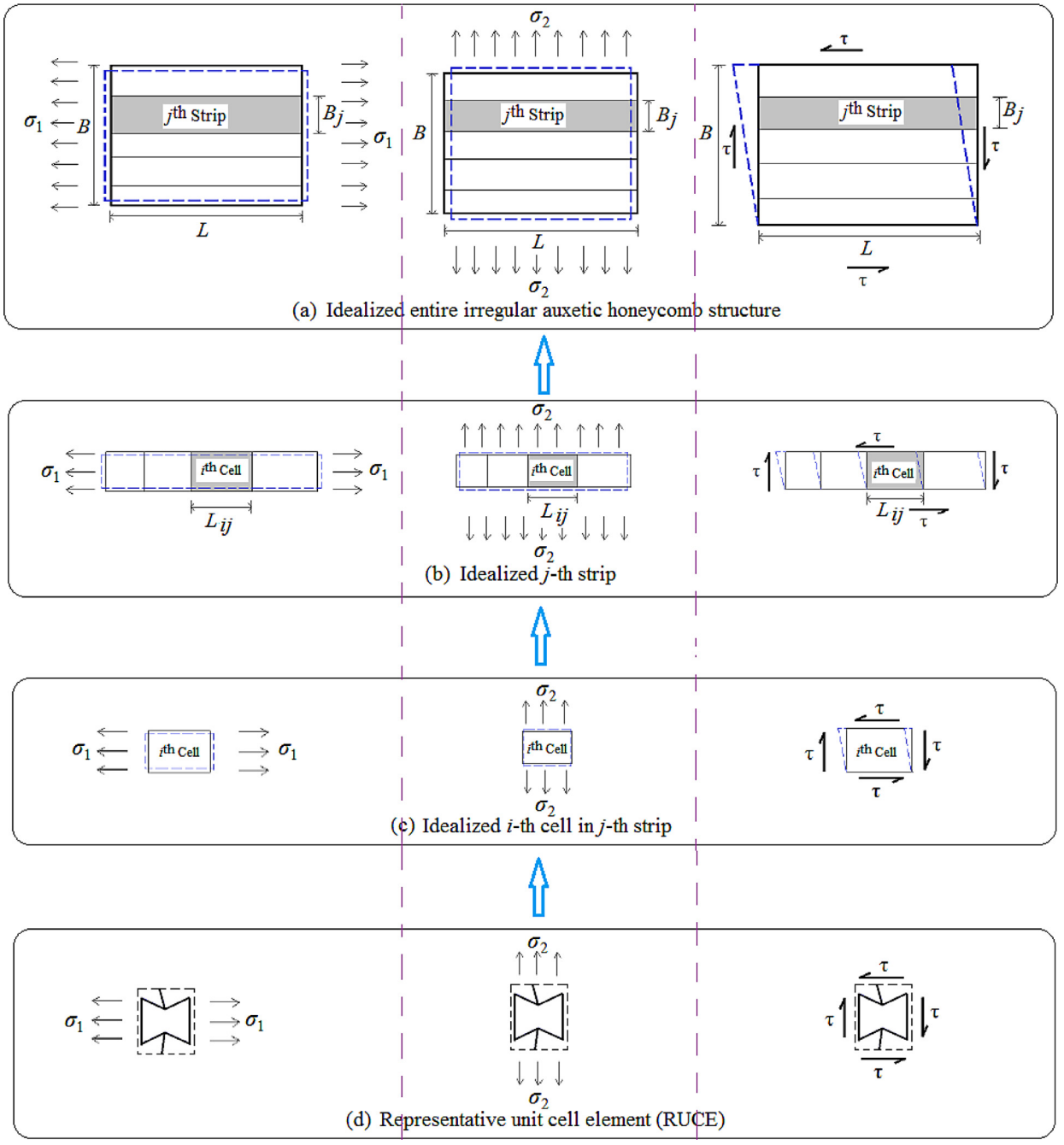

Fig. 6. Idealization of RUCE and proposed bottom up approach for propagation of the effect of irregularity from elementary level to global level.

where θ_{ij} is the inclination angle of the cell walls having length l_{ij} in the RUCE positioned at (i, j). In the next step, expression of equivalent longitudinal Young's modulus for a single strip ($\hat{E_{1j}}$) is utilized to obtain equivalent longitudinal Young's modulus of the entire irregular auxetic honeycomb structure (E_{1eq}) using force equilibrium and deformation compatibility conditions as follows.

$$\sigma_1 B b = \sum_{j=1}^{n} \sigma_{1j} B_j b \tag{35}$$

where B_j is the dimension of jth strip in direction-2 and $B = \sum_{j=1}^{n} B_j$. b represents the depth of honeycomb.

As strains in direction-1 for each of the n strips are same to satisfy the deformation compatibility condition, Eq. (35) leads to

$$\left(\sum_{j=1}^{n} B_j\right) E_{1eq} = \sum_{j=1}^{n} \hat{E_{1j}} B_j \tag{36}$$

Using Eqs. (34) and (36), equivalent Young's modulus in direction-1 of the entire irregular honeycomb structure

(E_{1eq}) can be expressed as

$$E_{1eq} = \frac{1}{\sum_{j=1}^{n} B_j} \sum_{j=1}^{n} \left(\frac{\sum_{i=1}^{m} l_{ij} \cos\theta_{ij}}{\sum_{i=1}^{m} \frac{l_{ij} \cos\theta_{ij}}{E_{1Uij}}} \right) B_j \tag{37}$$

where Young's modulus in direction-1 of a RUCE positioned at (i, j) is E_{1Uij}, which can be obtained from Eq. (5).

2.2.2. Transverse Young's modulus (E_{2eq})

To derive the expression of equivalent transverse Young's modulus for the entire irregular auxetic honeycomb structure (E_{2eq}), the transverse Young's moduli for the constituting RUCEs (E_{2U}) are assembled as discussed below. For obtaining E_{2eq}, stress σ_2 is applied in direction-2 as shown in the group of loading direction-2 (refer Fig. 6). If the force equilibrium under the application of stress σ_2 of j^{th} strip is considered,

$$\sigma_2 \left(\sum_{i=1}^{m} 2 l_{ij} \cos\theta_{ij} \right) b = \left(\sum_{i=1}^{m} \sigma_{2ij} 2 l_{ij} \cos\theta_{ij} \right) b \tag{38}$$

By deformation compatibility condition, strains of each RUCE in direction-2 of the jth strip are same. Eq. (38), rewritten as

$$\hat{E_{2j}} \left(\sum_{i=1}^{m} l_{ij} \cos\theta_{ij} \right) \epsilon = \left(\sum_{i=1}^{m} E_{2Uij} l_{ij} \cos\theta_{ij} \epsilon_{ij} \right) \tag{39}$$

where $\epsilon_{ij} = \epsilon$, for $i = 1, 2 \ldots m$ in the jth strip. $\hat{E_{2j}}$ is the equivalent elastic modulus in direction-2 of the jth strip.

$$\hat{E_{2j}} = \frac{\sum_{i=1}^{m} E_{2Uij} l_{ij} \cos\theta_{ij}}{\sum_{i=1}^{m} l_{ij} \cos\theta_{ij}} \tag{40}$$

Total deformation of the entire honeycomb in direction-2 (Δ_2) is the sum of deformations of each strips in that direction,

$$\Delta_2 = \sum_{j=1}^{n} \Delta_{2ij} \tag{41}$$

The Eq. (41) can be rewritten as

$$\epsilon_2 B = \sum_{j=1}^{n} \epsilon_{2j} B_j \tag{42}$$

where ϵ_2, ϵ_{2j} and B_j represent total strain of the entire honeycomb structure in direction-2, strain of jth strip in direction-2 and dimension in direction-2 of jth, strip, respectively.

Eq. (42) can be rewritten as

$$\frac{\sigma_2 \sum_{j=1}^{n} B_j}{E_{2eq}} = \sum_{j=1}^{n} \frac{\sigma_2 B_j}{\hat{E_{2j}}} \tag{43}$$

From Eqs. (40) and (43), the Young's modulus in direction-2 of the entire irregular honeycomb structure can be expressed as

$$E_{2eq} = \frac{1}{\left(\sum_{j=1}^{n} B_j \frac{\sum_{i=1}^{m} l_{ij} \cos\theta_{ij}}{\sum_{i=1}^{m} E_{2Uij} l_{ij} \cos\theta_{ij}} \right)} \sum_{j=1}^{n} B_j \tag{44}$$

where Young's modulus in direction-2 of a RUCE positioned at (i, j) is E_{2Uij}, which can be obtained from Eq. (15).

2.2.3. Poisson's ratio ν_{12eq}

To derive the expression of equivalent Poisson's ratio for loading direction-1 of the entire irregular auxetic honeycomb structure (ν_{12eq}), the Poisson's ratios for the constituting RUCEs (ν_{12U}) are assembled as discussed below. For obtaining ν_{12eq}, stress σ_1 is applied, similar to the derivation of E_{1U} (as shown in Fig. 6). If the application of stress σ_1 in the jth strip is considered, total deformation of the jth strip in direction-1 is summation of individual deformations of the RUCEs in direction-1 of that particular strip. Thus from Eq. 32, using the basic definition of ν_{12},

$$-\frac{\epsilon_2}{\hat{\nu}_{12j}} L = -\sum_{i=1}^{m} \frac{\epsilon_{2ij} L_{ij}}{\nu_{U12ij}} \tag{45}$$

where ϵ_2 and ϵ_{2ij} are the strains in direction-2 of jth strip and individual RUCEs of jth, strip respectively. ν_{U12ij} represents the Poisson's ratio for loading direction-1 of a RUCE positioned at (i, j). $\hat{\nu}_{12j}$ denotes the equivalent Poisson's ratio for loading direction-1 of the jth strip. To ensure the deformation compatibility condition $\epsilon_2 = \epsilon_{2ij}$ for $i = 1, 2, \ldots, m$ in the jth strip. Thus Eq. (45) leads to

$$\hat{\nu}_{12j} = \frac{L}{\sum_{i=1}^{m} \frac{L_{ij}}{\nu_{12Uij}}} \tag{46}$$

Total deformation of the entire honeycomb structure in direction-2 under the application of stress σ_1 along the two opposite edges parallel to direction-2 is summation of the individual deformations in direction-2 of n number of strips. Thus

$$\epsilon_2 B = \sum_{j=1}^{n} \epsilon_{2j} B_j \tag{47}$$

Using the basic definition of ν_{12} Eq. (47) becomes

$$\nu_{12eq} \epsilon_1 B = \sum_{j=1}^{n} \nu_{12j} \epsilon_{1j} B_j \tag{48}$$

where ν_{12eq} represents the equivalent Poisson's ratio for loading direction-1 of the entire irregular auxetic honeycomb structure. ϵ_1 and ϵ_{1j} denote the strain of entire honeycomb structure in direction-1 and strain of jth strip in direction-1, respectively.

From the condition of deformation comparability $\epsilon_1 = \epsilon_{1j}$ for $j = 1, 2, \ldots, n$. Thus from Eqs. (46) and (48),

$$\nu_{12eq} = \frac{1}{\sum_{j=1}^{n} B_j} \sum_{j=1}^{n} \left(\frac{\sum_{i=1}^{m} l_{ij} \cos\theta_{ij}}{\sum_{i=1}^{m} \frac{l_{ij} \cos\theta_{ij}}{\nu_{12Uij}}} \right) B_j \tag{49}$$

where ν_{12Uij} can be obtained from Eq. (18).

2.2.4. Poisson's ratio ν_{21eq}

To derive the expression of equivalent Poisson's ratio for loading direction-2 of the entire irregular auxetic honeycomb structure (ν_{21eq}), the Poisson's ratios for the constituting RUCEs (ν_{21U}) are assembled as discussed below. For obtaining ν_{21eq}, stress σ_2 is applied in direction-2, similar to the derivation of E_{2U} (as shown in Fig. 6). If the application of stress σ_2 in the jth strip is considered, total deformation of the jth strip in direction-1 is summation of

individual deformations of the RUCEs in direction-1 of that particular strip. Thus,

$$\epsilon_1 L = \sum_{i=1}^{m} \epsilon_{1ij} L_{ij} \tag{50}$$

Using the basic definition of ν_{21} Eq. (50) leads to

$$\hat{\nu}_{21j} \epsilon_2 L = \sum_{i=1}^{m} \nu_{21Uij} \epsilon_{2ij} L_{ij} \tag{51}$$

where $\hat{\nu}_{21j}$ represents the equivalent Poisson's ratio for loading direction-2 of the jth strip. ϵ_2 and ϵ_{2ij} are the strains in direction-2 of jth strip and individual RUCEs of jth strip, respectively. ν_{21Uij} represents the Poisson's ratio for loading direction-2 of a RUCE positioned at (i, j). To ensure the deformation compatibility condition $\epsilon_2 = \epsilon_{2ij}$ for $i = 1, 2, \ldots, m$ in the jth strip. Thus Eq. (51) leads to

$$\hat{\nu_{21j}} = \frac{\sum_{i=1}^{m} \nu_{21Uij} l_{ij} \cos\theta_{ij}}{\sum_{i=1}^{m} l_{ij} \cos\theta_{ij}} \tag{52}$$

Total deformation of the entire honeycomb structure in direction-2 under the application of stress σ_2 along the two opposite edges parallel to direction-1 is summation of the individual deformations in direction-2 of n number of strips. Thus

$$\epsilon_2 B = \sum_{j=1}^{n} \epsilon_{2j} B_j \tag{53}$$

By definition of ν_{21} Eq. (53) leads to

$$\frac{\epsilon_1}{\nu_{21eq}} B = \sum_{j=1}^{n} \frac{\epsilon_{1j}}{\hat{\nu_{21j}}} B_j \tag{54}$$

From the condition of deformation comparability $\epsilon_1 = \epsilon_{1j}$ for $j = 1, 2, \ldots, n$. Thus the equivalent Poisson's ratio for loading direction-2 of the entire irregular honeycomb structure

$$\nu_{21eq} = \frac{1}{(\sum_{j=1}^{n} B_j \frac{\sum_{i=1}^{m} l_{ij} \cos\theta_{ij}}{\sum_{i=1}^{m} \nu_{21Uij} l_{ij} \cos\theta_{ij}})} \sum_{j=1}^{n} B_j \tag{55}$$

where ν_{21Uij} can be obtained from Eq. (23).

2.2.5. Poisson's ratio (G_{12eq})

To derive the expression of equivalent shear modulus of the entire irregular honeycomb structure (G_{12eq}), the shear moduli for the constituting RUCEs (G_{12U}) are assembled as discussed below. For obtaining G_{12eq}, shear stress τ is applied as shown in Fig. 6). If the equilibrium of forces for application of stress τ in the jth strip is considered,

$$\tau L = \sum_{i=1}^{m} \tau_{ij} L_{ij} \tag{56}$$

By definition of shear modulus Eq. (56) can be rewritten as

$$\hat{G}_{12j} \gamma L = \sum_{i=1}^{m} G_{12Uij} \gamma_{ij} L_{ij} \tag{57}$$

where $\hat{G}_{12j}$ represents the equivalent shear modulus of the jth strip. γ and γ_{ij} are the shear strains of jth strip and individual RUCEs of the jth strip, respectively. G_{12Uij} represents the shear modulus of a RUCE positioned at (i, j). To ensure the deformation compatibility condition $\gamma = \gamma_{ij}$ for $i = 1, 2, \ldots, m$ in the jth strip. Thus Eq. (57) leads to

$$\hat{G}_{12j} = \frac{\sum_{i=1}^{m} G_{12Uij} l_{ij} \cos\theta_{ij}}{\sum_{i=1}^{m} l_{ij} \cos\theta_{ij}} \tag{58}$$

Total lateral deformation of one edge compared to the opposite edge of the entire honeycomb structure under the application of shear stress τ is the summation of the individual lateral deformations of n number of strips. Thus

$$\gamma B = \sum_{j=1}^{n} \gamma_j B_j \tag{59}$$

By definition of G_{12} Eq. (59) leads to

$$\frac{\tau}{G_{12eq}} B = \sum_{j=1}^{n} \frac{\tau_j}{\hat{G_{12j}}} B_j \tag{60}$$

From Eqs. (58) and (60), equivalent shear modulus of the entire irregular auxetic honeycomb structure can be expressed as

$$G_{12eq} = \frac{1}{(\sum_{j=1}^{n} B_j \frac{\sum_{i=1}^{m} l_{ij} \cos\theta_{ij}}{\sum_{i=1}^{m} G_{12Uij} l_{ij} \cos\theta_{ij}})} \sum_{j=1}^{n} B_j \tag{61}$$

where G_{12Uij} can be obtained from Eq. (30).

The closed-form formulae of elastic moduli for irregular auxetic honeycombs have been summarized in Table 1, for ready reference to the readers. It is worthy to note here that the formulae derived in this article for irregular auxetic honeycombs reduce to the expressions provided by Gibson and Ashby (1999) in case of uniform honeycombs (i.e. $B_1 = B_2 = \cdots = B_n$; $s = h/2$; $\alpha = \beta = 90^\circ$; $l_{ij} = l$ and $\theta_{ij} = -\theta$, for all i and j).

3. Finite element modelling and validation

A highly generalized finite element code has been developed using Matlab (MATLAB, 2013) to obtain the in-plane elastic moduli numerically for honeycombs having spatially random structural variation. The developed finite element code is capable of accepting the number of RUCEs in direction-1 and 2 as input in addition to material properties and other random geometrical features to obtain corresponding five elastic moduli as output. Purpose of the finite element model in the present study is to validate the proposed analytical approach for obtaining in-plane elastic moduli of irregular auxetic honeycombs. Each cell wall has been modelled as an Euler–Bernoulli beam element neglecting axial and shear deformation with the assumption of high axial rigidity and low cell wall thickness, respectively.

The finite element model has been validated with results from available literature (Gibson and Ashby, 1999). Representative results for validation are furnished in Fig. 7 for a regular auxetic honeycomb with cell angle 30° and h/l ratio of 1. Non-dimensional elastic moduli have been plotted using: $E_1 \rightarrow \frac{E_1}{E_s} \times 10^5$, $E_2 \rightarrow \frac{E_2}{E_s} \times 10^5$, $\nu_{12} \rightarrow \nu_{12}$, $\nu_{21} \rightarrow \nu_{21}$ and $G_{12} \rightarrow \frac{G_{12}}{E_s} \times 10^6$ respectively, for the ease

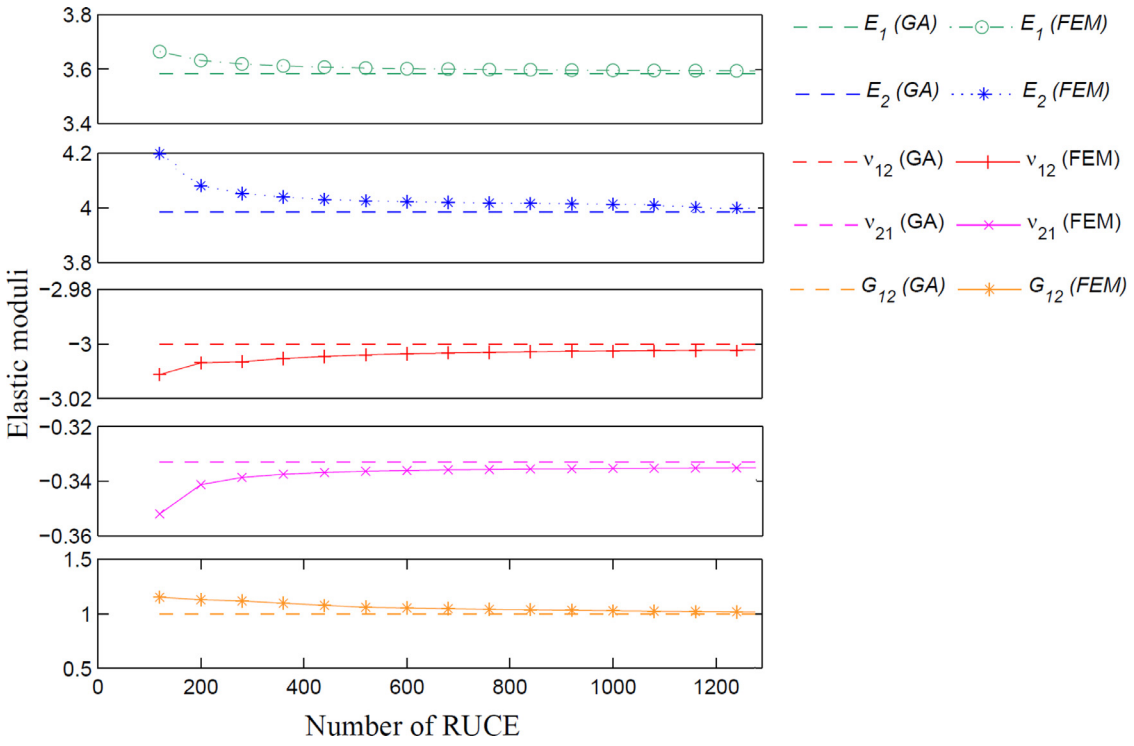

Fig. 7. Convergence study and validation of finite element model for obtaining elastic moduli of auxetic honeycomb (Here GA and FEM denote the results obtained by the formulae provided by Gibson and Ashby (1999) and the developed finite element code respectively for regular auxetic honeycomb).

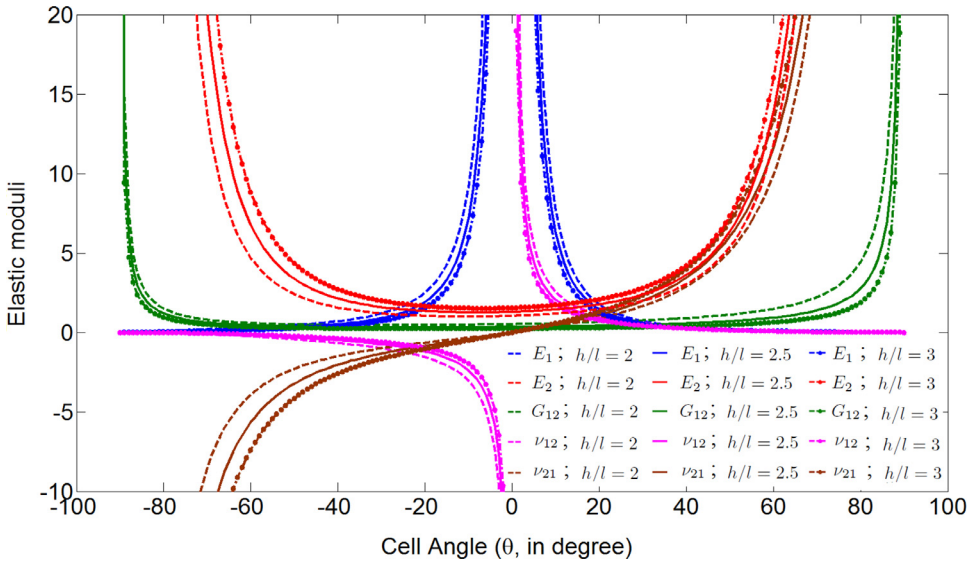

Fig. 8. Variation of different non-denominational elastic moduli with cell angle (θ) for regular honeycombs ($\Delta\theta = 0^{\circ}$).

of understanding the convergence and validation study. It should be noted here that θ value referred in this study is accordance with Fig. 3(a), meaning by $\theta = -30^{\circ}$ as per the formulation presented in Gibson and Ashby (1999). Here convergence studies have been carried out for the five in-plane elastic moduli with different number of RUCE to ensure the average global behaviour of the entire honeycomb by avoiding any localised deformation due to boundary effect. In the present study, the number of RUCE has been adopted as 961 for all the subsequent analyses to comprehensively capture the effect of random irregularity, which is the emphasis of this work. As considering very less number of RUCEs for analysis may fail to portray the effect of randomness in the global structural behaviour, a relatively larger size of lattice is adopted.

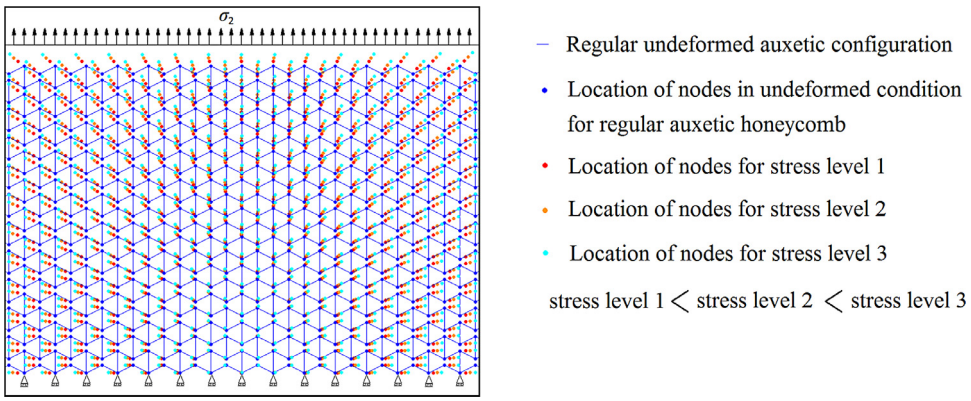

Fig. 9. Typical location of nodes for a regular auxetic honeycomb ($\theta = 45^\circ$; $\Delta\theta = 0^\circ$; $h/l = 2$) under the application of stresses with different levels in direction-2.

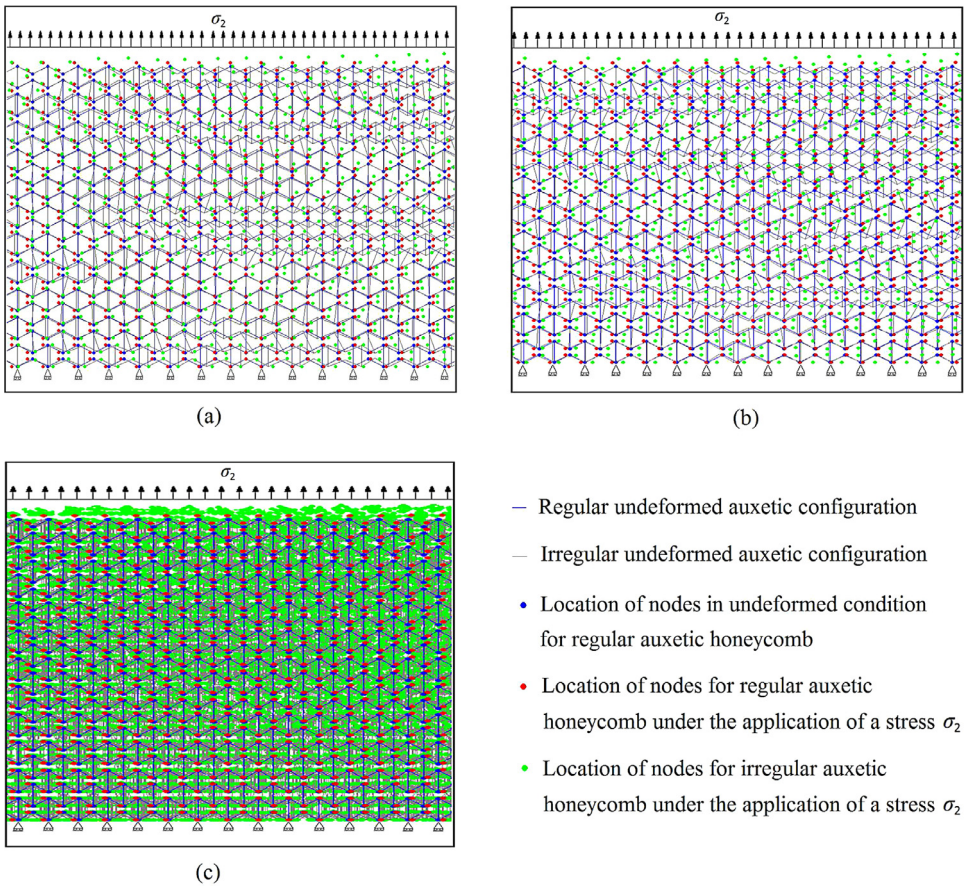

Fig. 10. Typical representation of irregular auxetic honeycombs ($\theta = 45^\circ$; $\Delta\theta = 5^\circ$; $h/l = 2$) along with location of nodes under the application of stress in direction-2.

4. Results and discussion

The analytical approach proposed in this study is capable of obtaining equivalent in-plane elastic properties for irregular auxetic honeycombs from known spatial distribution of cell angle and material properties of the honeycomb cell walls. Such irregularities in auxetic material can be characterized by using common techniques like digital image analysis. For the purpose of finding the range of variation in elastic moduli due to spatial uncertainty, cell angles and material properties can be perturbed following a random distribution within specific bounds. From the expressions of effective elastic moduli derived in Section 2, it is evident that the five elastic moduli depend on the ratios h/l, t/l, s/l and the angles θ, α, β (refer Table 1). In addition to these quantities, the two Young's moduli and shear

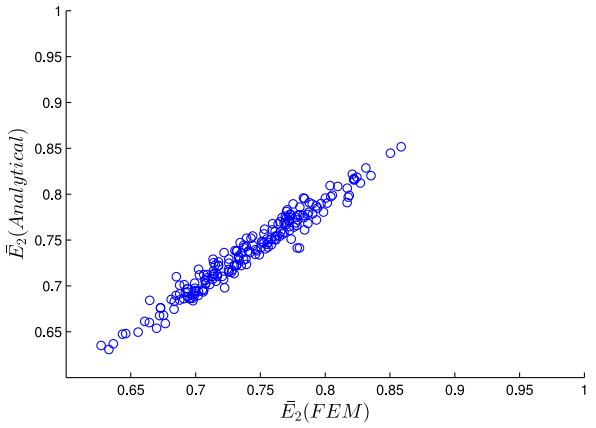

(a) Scatter plot for E_2

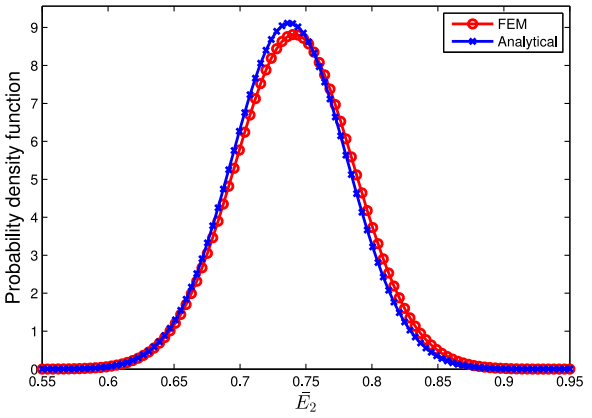

(a) Probability density function E_2

Fig. 11. Typical results for validation of proposed analytical approach with respect to direct finite element simulation results for E_2 with $\theta = 45^\circ$, $\Delta\theta = 5^\circ$ (ratio of E_2 for irregular honeycomb and regular honeycomb is presented).

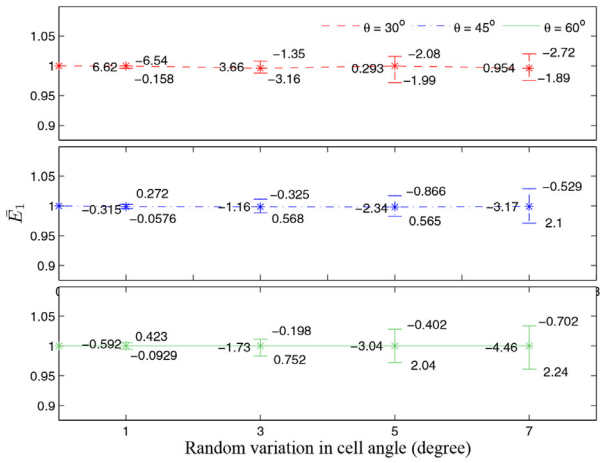

(a) $h/l = 2$

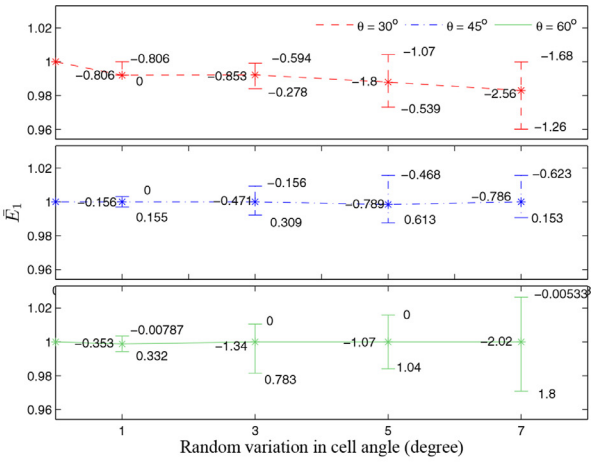

(b) $h/l = 2.5$

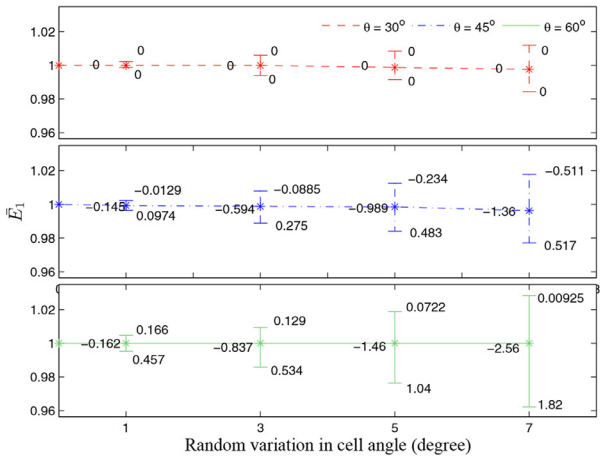

(c) $h/l = 3$

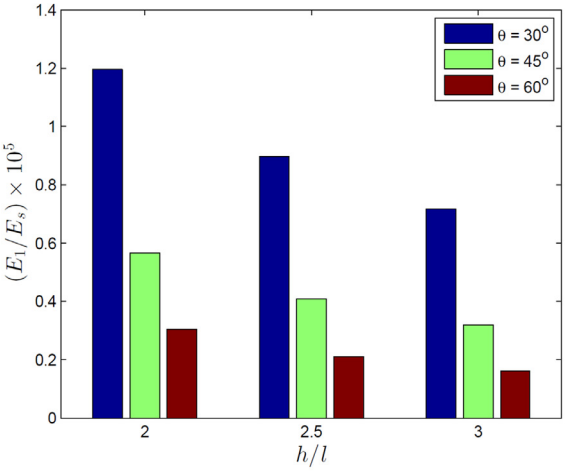

(d) Regular auxetic honeycomb

Fig. 12. Effect of structural irregularity on non-dimensional E_1.

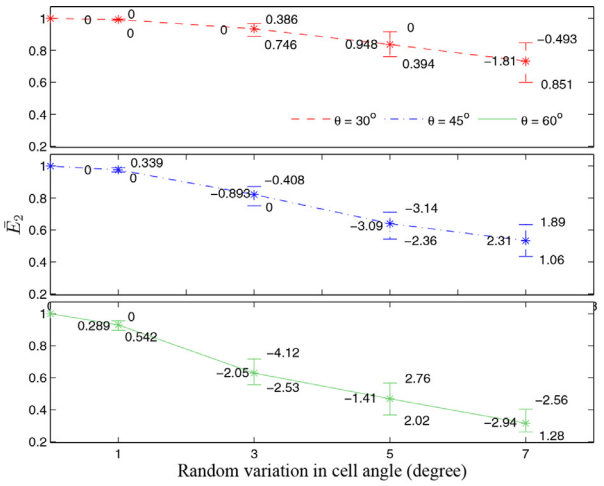

(a) $h/l = 2$

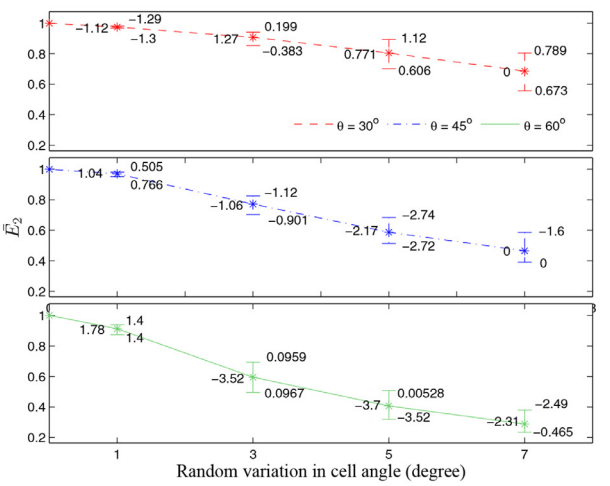

(b) $h/l = 2.5$

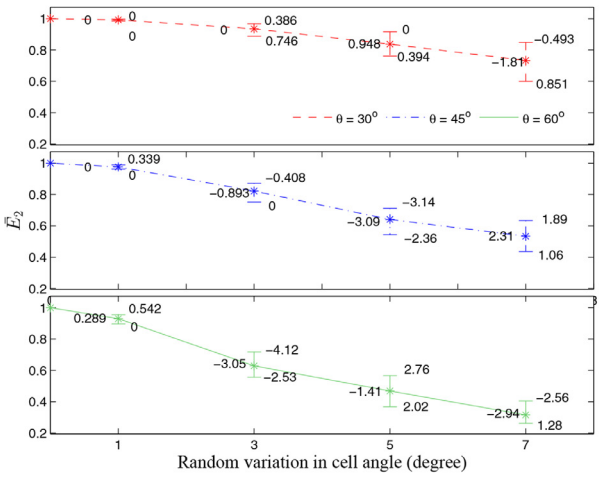

(c) $h/l = 3$

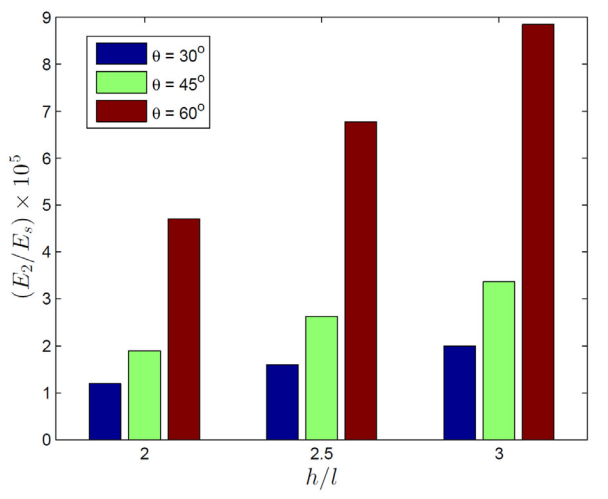

(d) Regular auxetic honeycomb

Fig. 13. Effect of structural irregularity on non-dimensional E_2.

modulus also depend on E_s. Only bending deformation has been accounted in the present analysis as the effect due to axial and shear deformation becomes negligible for very high axial rigidity and small value of the ratio t/l, respectively. The formulations presented in Section 2 are valid for small strain allowing the non-linearity due to beam-column effect to be neglected.

In the present analysis, results have been presented for three different h/l ratios, namely: 2, 2.5 and 3 with a very small t/l value ($\sim 10^{-2}$) to portray the effect of random variation in cell angles. For each of these h/l ratios, three different cell angles have been considered, namely: 30°, 45° and 60°. Deterministic results ($\Delta\theta = 0^\circ$) for the five in-plane elastic moduli are presented in Fig. 8 considering the variation of cell angle in the entire domain. Non-dimensional elastic moduli have been plotted following: $E_1 \to \frac{E_1}{E_s} \times 10^5$, $E_2 \to \frac{E_2}{E_s} \times 10^5$, $\nu_{12} \to \nu_{12}$, $\nu_{21} \to \nu_{21}$ and $G_{12} \to \frac{G_{12}}{E_s} \times 10^6$ respectively, for the ease of a comparative assessment. The figure caters to interesting insights on rate of changes in the values of different elastic moduli with the variation of cell angle and h/l ratio. This in turn, provides an idea about the relative sensitivity of the elastic moduli to changes in cell angle at different points. In this article, results are furnished for spatial irregularity in the cell angles only. The maximum, minimum and mean values of non-dimensional in-plane elastic moduli for different degree of spatially random variations in cell angles ($\Delta\theta = 0^\circ, 1^\circ, 3^\circ, 5^\circ, 7^\circ$) are shown in Figs. 12–16. In each of these figures, subfigures (a)–(c) show the effect of irregularity on different in-plane elastic modulus, wherein the ratios $\bar{Z}(= \frac{Z_{irregular}}{Z_{regular}})$ are presented (Z denotes a particular elastic modulus and the subscripts irregular and regular indicate the values of effective elastic moduli

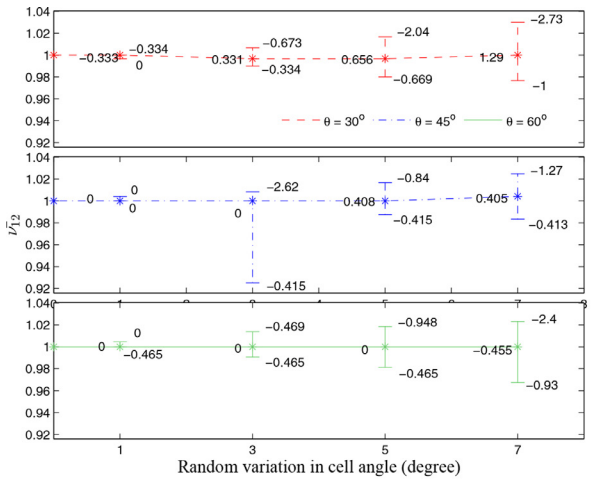

(a) $h/l = 2$

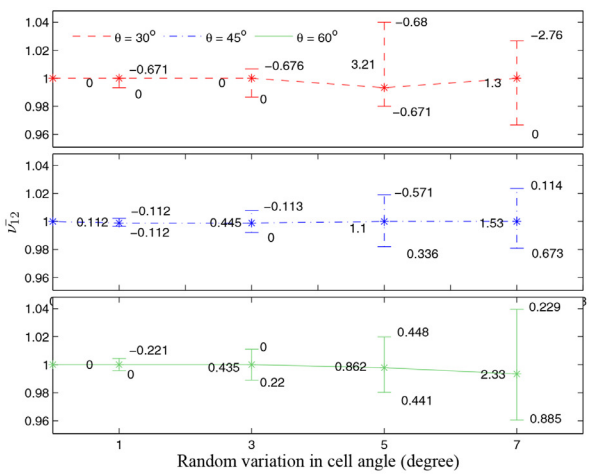

(b) $h/l = 2.5$

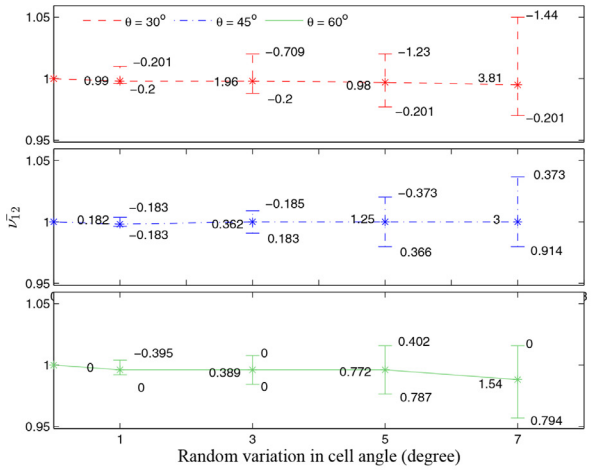

(c) $h/l = 3$

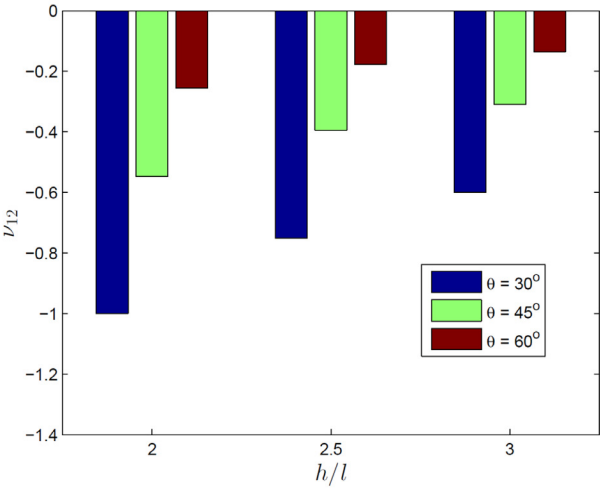

(d) Regular auxetic honeycomb

Fig. 14. Effect of structural irregularity on non-dimensional ν_{12}.

of irregular auxetic honeycomb and regular auxetic honeycomb respectively) for different degree of randomness in cell angles. The numerical values shown in the right side of each '**I**' shaped marks represent percentage errors in the maximum and minimum values of elastic moduli calculated using the proposed analysis compared to the finite element results. The numerical values shown in the left side represent the same for the mean values. Smaller values in the percentage errors would indicate that the proposed analytical approach is capable of obtaining in-plane elastic moduli for irregular auxetic honeycombs with high precision. Points on the Y-axis depicts the values of elastic moduli corresponding to perfectly periodic cell structure (i.e.$\Delta\theta = 0$). Subfigure (d), in each of the figures of Figs. 12–16 show elastic moduli of regular honeycombs. For a particular cell angle θ, results have been obtained using a set of uniformly distributed 10, 000 random samples in the range of $[\theta - \Delta\theta, \theta + \Delta\theta]$. The set of input parameter for a particular sample consists of N number of cell angles in the specified range, where $N(= n \times m)$ is the total number of RUCEs in the entire irregular honeycomb structure. In the present analysis t, s and E_s have been modelled to possess no spatial variation. The quantities h and θ have been considered as the two random input parameters following uniform distribution, while α and β are dependent features.

Typical location of nodes for a regular auxetic honeycomb under the application of stresses with different levels is shown in Fig. 9. Movement of the nodes for a particular stress level are higher as the distance from support increases due to a cumulative effect. It can also be noticed that movement of the nodes are higher in direction 2 for higher level of stresses, as expected. Another interesting observation from the figure is that deformed

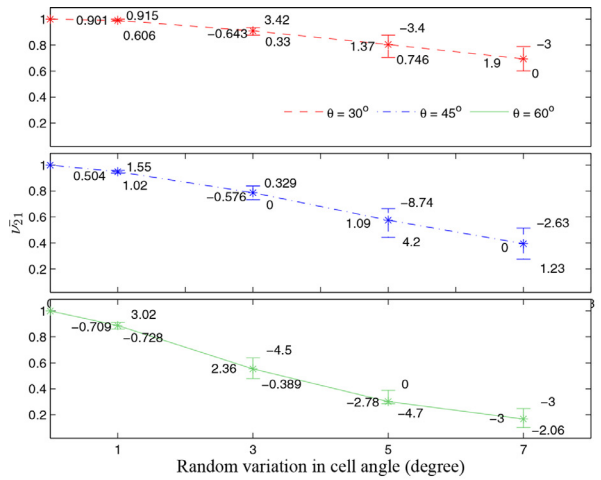

(a) $h/l = 2$

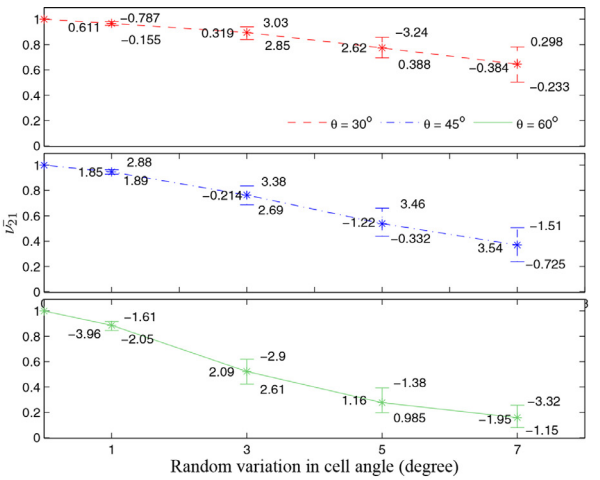

(b) $h/l = 2.5$

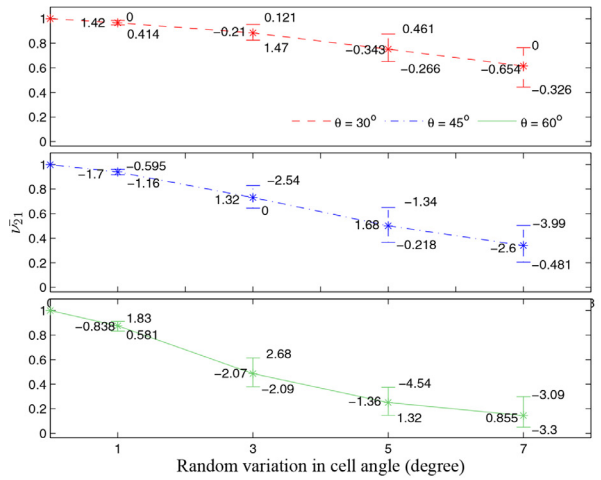

(c) $h/l = 3$

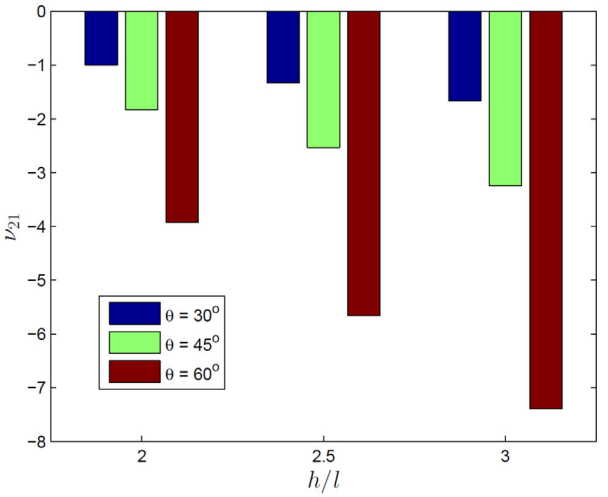

(d) Regular auxetic honeycomb

Fig. 15. Effect of structural irregularity on non-dimensional ν_{21}.

location of the nodes allow the lattice to expand in both direction 1 and 2 under the application of tensile stress σ_2 conforming auxetic property of the honeycomb. Location of nodes for the deformed honeycombs can be visualized relative to undeformed shape of the respective regular configuration ($\theta = 45^\circ$; $h/l = 2$). Fig. 10 presents typical irregular auxetic honeycombs for different random configurations along with location of nodes under the application of stress in direction-2. Fig. 10(a) and (b) show the movement of nodes for two random irregular auxetic configurations respectively (corresponding to two different random cell geometries), while Fig. 10(c) presents the bound of movements for different nodes in randomly irregular auxetic honeycombs considering 10,000 random cell configurations. It can be noticed from the figures that movement of the nodes in direction 2 increases considerably for randomly irregular structural geometries compared to the regular configuration. This, in turn indicates reduction in E_2 due to the effect of irregularity, which agrees well with the results presented (Fig. 13) later in this section.

A representative scatter plot for E_2 showing accuracy of the proposed analytical formulae is furnished in Fig. 11(a), wherein low deviation of the points from diagonal line affirms high level of precision with respect to finite element results for irregular auxetic honeycomb. Fig. 11(b) shows probability density functions for E_2 of irregular auxetic honeycomb, wherein low deviation between results of the analytical methodology and finite element method corroborates high level of precision of the proposed approach. It is interesting to notice here that, even though the cell angles of an irregular honeycomb sample have been drawn from an uniform distribution, the elastic moduli of irregular honeycombs follow Gaussian distribution.

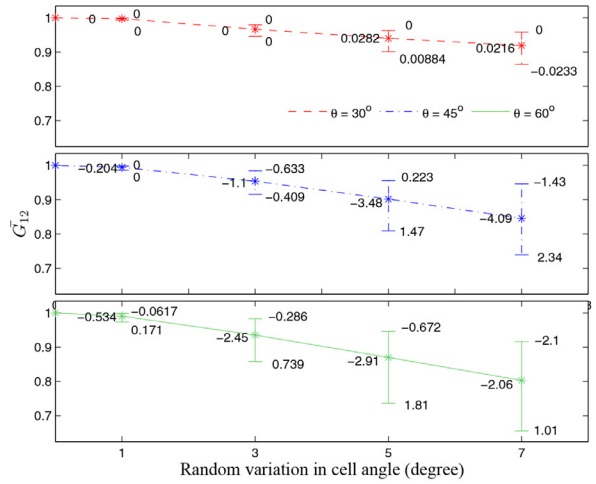

(a) $h/l = 2$

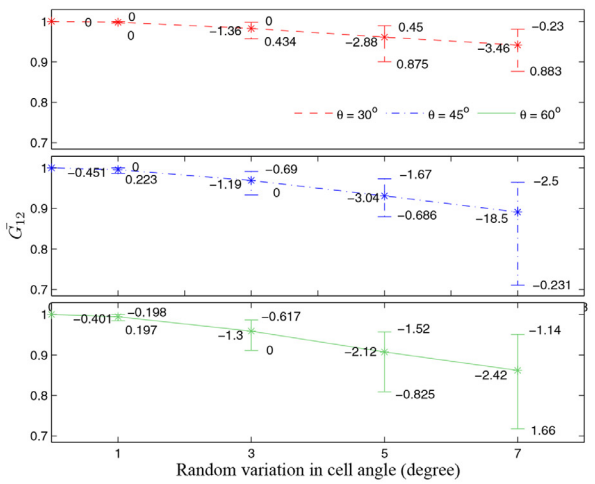

(b) $h/l = 2.5$

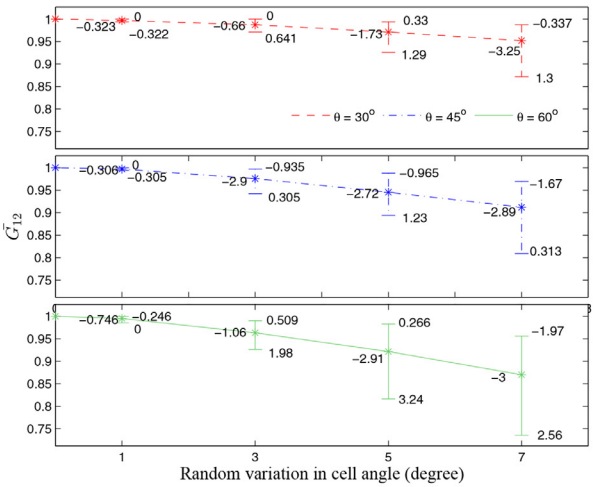

(c) $h/l = 3$

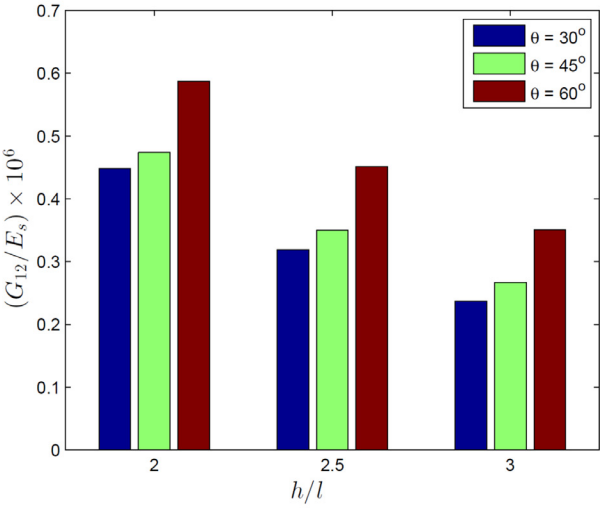

(d) Regular auxetic honeycomb

Fig. 16. Effect of structural irregularity on non-dimensional G_{12}.

Figs. 12–16 show the effect of spatially random variation of cell angles in the elastic moduli of irregular auxetic honeycomb. From the figures it is evident that irregularity in the cell angles have negligible influence in the mean values of E_1 and ν_{12}, whereas mean values of E_2, ν_{21} and G_{12} reduce significantly with increasing degree of random variation in cell angle. Thus the auxetic property of honeycomb is found to reduce considerably for ν_{21} with the increase in degree of structural irregularity. The range of variations of all the elastic moduli are found to increase with increasing degree of irregularity in cell angles, as expected. The highest rates of reduction in the values of E_2, ν_{21} and G_{12} with the increase in degree of irregularity are noticed for mean cell angle of 60°, followed by 45° and 30°. It is worthy to mention here that, the percentage errors presented in the figures indicate the results obtained using the proposed computationally efficient analytical approach are in good agreement with that of finite element method.

Previous investigations in the field of honeycomb structure have dealt with the effect of under-expansion and over-expansion of cells (Papka and Kyriakides, 1994) in non-auxetic hexagonal honeycomb with regular configuration using numerical and experimental studies. The present investigation shows the effects of spatially random distribution of under and over expanded cells of different degree on elastic moduli for irregular auxetic honeycomb structure. Liu et al. (2014) have reported based on limited number of samples using finite element simulation that structural irregularity in auxetic honeycombs tends to lower the effective in-plane elastic moduli and auxetic property of the system. This observation is similar to the inference drawn in the present article, which uses an efficient analytical approach. Noteworthy is the fact that it is

Table 1
Summary of formulae for effective in-plane elastic properties of irregular auxetic honeycombs.

Parameter	In-plane elastic properties					
	E_1	E_2	ν_{12}	ν_{21}	G_{12}	
Representative unit cell element (RUCE)	$E_{1U} = E_s\left(\frac{t}{l}\right)^3 \frac{\cos\theta}{\left(\frac{h}{l}-\sin\theta\right)\sin^2\theta}$	$E_{2U} = E_s\left(\frac{t}{l}\right)^3 \frac{\left(\frac{h}{l}+2\frac{s}{l}-2\sin\theta\right)}{\cos\theta\left(2\cos^2\theta+8\left(\frac{s}{l}\right)^3\left(\frac{\cos^2\alpha}{\sin\alpha}+\frac{\cos^2\beta}{\sin\beta}\right)+2\left(\frac{s}{l}\right)^2(\cot^2\alpha+\cot^2\beta)\right)}$	$\nu_{12U} = -\frac{2\cos^2\theta}{\left(-2\sin\theta+2\frac{s}{l}+\frac{h}{l}\right)\sin\theta}$	$\nu_{21U} = -\frac{\sin\theta\left(\frac{h}{l}+2\frac{s}{l}-2\sin\theta\right)}{2\cos^2\theta+8\left(\frac{s}{l}\right)^3\left(\frac{\cos^2\alpha}{\sin\alpha}+\frac{\cos^2\beta}{\sin\beta}\right)+2\left(\frac{s}{l}\right)^2(\cot^2\alpha+\cot^2\beta)}$	$G_{12U} = E_s\left(\frac{t}{l}\right)^3 \frac{\left(2\frac{s}{l}+\frac{h}{l}-2\sin\theta\right)}{2\cos\theta\left(2\left(\frac{s}{l}\right)^2+4\left(\frac{s}{l}\right)^3\left(\frac{1}{\sin\alpha}+\frac{1}{\sin\beta}\right)+\frac{1}{2}\left(\frac{s}{l}\right)^3+\left(\frac{s}{l}-\sin\theta\right)\left(\frac{h}{l}\right)^2\right)}$
Entire irregular auxetic honeycomb	$E_{1eq} = \frac{1}{\sum_{j=1}^{n} B_j}\sum_{j=1}^{n}\left(\frac{\sum_{i=1}^{m} l_{ij}\cos\theta_{ij}}{\sum_{i=1}^{m}\frac{l_{ij}\cos\theta_{ij}}{E_{1U(ij)}}}\right)B_j$	$E_{2eq} = \frac{1}{\left(\sum_{j=1}^{n} B_j\right)}\frac{\sum_{i=1}^{m} l_{ij}\cos\theta_{ij}}{\sum_{i=1}^{m}\frac{l_{ij}\cos\theta_{ij}}{E_{2U(ij)}}}\sum_{j=1}^{n} B_j$	$\nu_{12eq} = \frac{1}{\sum_{j=1}^{n} B_j}\sum_{j=1}^{n}\left(\frac{\sum_{i=1}^{m} l_{ij}\cos\theta_{ij}}{\sum_{i=1}^{m}\frac{l_{ij}\cos\theta_{ij}}{\nu_{12U(ij)}}}\right)B_j$	$\nu_{21eq} = \frac{1}{\left(\sum_{j=1}^{n} B_j\right)}\frac{\sum_{i=1}^{m} l_{ij}\cos\theta_{ij}}{\sum_{i=1}^{m}\frac{l_{ij}\cos\theta_{ij}}{\nu_{21U(ij)}}}\sum_{j=1}^{n} B_j$	$G_{12eq} = \frac{1}{\left(\sum_{j=1}^{n} B_j\right)}\frac{\sum_{i=1}^{m} l_{ij}\cos\theta_{ij}}{\sum_{i=1}^{m}\frac{l_{ij}\cos\theta_{ij}}{G_{12U(ij)}}}\sum_{j=1}^{n} B_j$

possible to characterize the effect of structural irregularity using a robust framework with adequate number of samples only because of the development of the computationally efficient analytical approach. In the proposed analysis of irregular auxetic honeycomb structure having spatially random variations in cell angles, the cell walls having inclination angles α and β play a vital role. As the range of random variation in cell angles ($\Delta\theta$) increases, the inclination angle with respect to direction-2 of these cell walls are also found to increase. Subsequently considering the bending stiffness of the cell walls having inclination angles α and β, the trends of different in-plane elastic moduli with variation in degree of randomness can be explained.

5. Conclusion

A novel bottom up analytical approach for predicting equivalent in-plane elastic moduli of auxetic honeycombs having spatial irregularities is presented in this article. In the proposed framework, effect of structural randomness is accounted by analysing the representative unit cell elements first and then the effect of irregularity is propagated towards the global properties of the entire structure using basic principles of mechanics following a multi-scale approach. Though there are few literature available dealing with different forms of irregularity in honeycombs, those are based on either experimental investigation or numerical simulation. Moreover such studies on auxetic honeycombs are very scarce. This article proposes an efficient analytical framework for auxetic honeycomb. The basic physics behind elastic deformation of irregular auxetic honeycombs as presented in this article being scale-independent, the present study is applicable across different length scales. The closed form expressions developed for longitudinal Young's modulus, transverse Young's modulus and shear modulus are functions of both structural geometry and material properties of irregular auxetic honeycombs, while the Poisson's ratios depend only on structural geometry. The results obtained using the proposed analytical method for spatially random variation of cell angles have been compared with those obtained from the direct finite element simulation. The mean and range of variation for different elastic moduli are found to be in good agreement. Equivalent elastic properties of irregular honeycombs can be obtained using the proposed analytical framework more efficiently compared to expensive finite element simulation approach without compromising the accuracy of results. An important finding of this study is that, though the effect of spatially random variations in cell angle on E_1 and ν_{12} is negligible, E_2, ν_{21} and G_{12} reduce significantly with the increase in degree of random variation of the cell angles. Thus the auxetic property of honeycomb reduces considerably for ν_{21} with the increase in degree of structural irregularity. This uncertainty in the elastic moduli of auxetic honeycombs owing to random variations in cell angle would have significant influence on the subsequent analysis and design process. The formulae developed here can also be used to predict equivalent in-plane elastic moduli of irregular auxetic honeycombs having spatial variation in material properties

and thickness of cell wall and therefore the closed form formulae can be used for efficient stochastic analysis of such material responses accounting different forms of irregularity and uncertainty associated with spatial distribution of intrinsic material properties and structural geometry. The proposed analytical framework to efficiently analyse irregular honeycombs can be extended further to other cellular structures considering appropriate representative unit cell element and the effect of axial and shear deformations can also be incorporated in such future investigations.

Acknowledgements

TM acknowledges the financial support from Swansea University through the award of Zienkiewicz Scholarship. SA acknowledges the financial support from The Royal Society of London through the Wolfson Research Merit award. The authors also gratefully acknowledge the valuable comments of Prof. Fabrizio Scarpa (University of Bristol) on this work during preparation of the manuscript.

References

Ajdari, A., Nayeb-Hashemi, H., Canavan, P., Warner, G., 2008. Effect of defects on elastic-plastic behavior of cellular materials. Mater. Sci. Eng.: A 487 (1–2), 558–567.

Alsayednoor, J., Harrison, P., Guo, Z., 2013. Large strain compressive response of 2-d periodic representative volume element for random foam microstructures. Mech. Mater. 66, 7–20.

Bacigalupo, A., Bellis, M.L.D., 2015. Auxetic anti-tetrachiral materials: equivalent elastic properties and frequency band-gaps. Compos. Struct. 131, 530–544.

Bacigalupo, A., Gambarotta, L., 2014. Homogenization of periodic hexa- and tetrachiral cellular solids. Compos. Struct. 116, 461–476.

Banerjee, S., 2014. On the mechanical properties of hierarchical lattices. Mech. Mater. 72, 19–32.

Critchley, R., Corni, I., Wharton, J.A., Walsh, F.C., Wood, R.J.K., Stokes, K.R., 2013. A review of the manufacture, mechanical properties and potential applications of auxetic foams. Phys. Status Solidi B 250 (10), 1963–1982.

Dey, S., Mukhopadhyay, T., Khodaparast, H.H., Kerfriden, P., Adhikari, S., 2015a. Rotational and ply-level uncertainty in response of composite shallow conical shells. Compos. Struct. 131, 594–605.

Dey, S., Mukhopadhyay, T., Sahu, S.K., Li, G., Rabitz, H., Adhikari, S., 2015b. Thermal uncertainty quantification in frequency responses of laminated composite plates. Compos. Part B: Eng. 80, 186–197.

Evans, K.E., Alderson, A., 2000. Auxetic materials: functional materials and structures from lateral thinking!. Adv. Mater. 12 (9), 617–628.

Evans, K.E., Nkansah, M.A., Hutchinson, I.J., Rogers, S.C., 1991. Molecular network design. Nature 353 (6340), 124.

Gereke, T., Malekmohammadi, S., ASCE, S.M., Nadot-Martin, C., Dai, C., Ellyin, F., Vaziri, R., 2012. Multiscale stochastic modeling of the elastic properties of strand-based wood composites. J. Eng. Mech. 138 (7), 791–799.

Gibson, L., Ashby, M.F., 1999. Cellular Solids Structure and Properties. Cambridge University Press, Cambridge, UK.

Grima, J.N., Cauchi, R., Gatt, R., Attard, D., 2013. Honeycomb composites with auxetic out-of-plane characteristics. Compos. Struct. 106, 150–159.

Grima, J.N., Winczewski, S., Mizzi, L., Grech, M.C., Cauchi, R., Gatt, R., Attard, D., Wojciechowski, K.W., ybicki, J.R., 2015. Tailoring graphene to achieve negative poisson's ratio properties. Adv. Mater. 27, 1455–1459.

Hurtado, J.E., Barbat, A.H., 1998. Monte carlo techniques in computational stochastic mechanics. Arch. Comput. Meth. Eng. 5 (1), 3–29.

Karnessis, N., Burriesci, G., 2013. Uniaxial and buckling mechanical response of auxetic cellular tubes. Smart Mater. Struct. 22 (8), 084008.

Li, K., Gao, X.L., Subhash, G., 2005. Effects of cell shape and cell wall thickness variations on the elastic properties of two-dimensional cellular solids. Int. J. Solids Struct. 42 (5–6), 1777–1795.

Li, K., Gao, X.L., Wang, J., 2007. Dynamic crushing behavior of honeycomb structures with irregular cell shapes and non-uniform cell wall thickness. Int. J. Solids Struct. 44 (14-15), 5003– 5026.

Liu, W., Wang, N., Huang, J., Zhong, H., 2014. The effect of irregularity, residual convex units and stresses on the effective mechanical properties of 2d auxetic cellular structure. Mater. Sci. Eng.: A 609, 26–33.

Malek, S., Gibson, L., 2015. Effectiveelastic properties of periodic hexagonal honeycombs. Mech. Mater. 91 (1), 226–240.

MATLAB, 2013. Version 8.2.0.701 (R2013b). The MathWorks Inc.

Mukhopadhyay, T., Adhikari, S., 2016. Equivalent in-plane elastic properties of irregular honeycombs: an analytical approach. Int. J. Solids Struct. doi:10.1016/j.ijsolstr.2015.12.006.

Nkansah, M.A., Evans, K.E., Hutchinson, I.J., 1994. Modelling the mechanical properties of an auxetic molecular network. Model. Simul. Mater. Sci. Eng. 2 (3), 337.

Overaker, D.W., Cuitiño, A.M., Langrana, N.A., 1998. Effects of morphology and orientation on the behavior of two-dimensional hexagonal foams and application in a re-entrant foam anchor model. Mech. Mater. 29 (1), 43–52.

Papka, S.D., Kyriakides, S., 1994. In-plane compressive response and crushing of honeycomb. J. Mech. Phys. Solids 42 (10), 1499–1532.

Rad, M.S., Prawoto, Y., Ahmad, Z., 2014. Analytical solution and finite element approach to the 3d re-entrant structures of auxetic materials. Mech. Mater. 74, 76–87.

Roark, R.J., Young, W.C., 1976. Formulas for Stress and Strain. McGraw-Hill Book Company.

Scarpa, F., Panayiotou, P., Tomlinson, G., 2000. Numerical and experimental uniaxial loading on in-plane auxetic honeycombs. J. Strain Anal. Eng. Des. 35 (5), 383–388.

Scarpa, F., Smith, F.C., Chambers, B., 2003. Mechanical and electromagnetic behaviour of auxetic honeycomb structures. Aeronaut. J. 107 (1069), 175–183.

Scarpa, F., Tomlin, P.J., 2000. On the transverse shear modulus of negative poisson's ratio honeycomb structures. Fatigue Fracture Eng. Mater. Struct. 23 (8), 717–720.

Scarpa, F., Tomlinson, G., 2000. Theoretical characteristics of the vibration of sandwich plates with in-plane negative poisson's ratio values. J. Sound Vib. 230 (1), 45–67.

Stavroulakis, G.E., 2005. Auxetic behaviour: appearance and engineering applications. Phys. Stat. Solidi (b) 242 (3), 710–720.

Sun, J., Gao, H., Scarpa, F., Lira, C., Liu, Y., Leng, J., 2014. Active inflatable auxetic honeycomb structural concept for morphing wingtips. Smart Materials and Structures 23 (12), 125023.

Triantafyllidis, N., Schraad, M.W., 1998. Onset of failure in aluminum honeycombs under general in-plane loading. J. Mech. Phys. Solids 46 (6), 1089–1124.

Wan, H., Ohtaki, H., Kotosaka, S., Hu, G., 2004. A study of negative poisson's ratios in auxetic honeycombs based on a large deflection model. Eur. J. Mech. - A/Solids 23 (1), 95–106.

Wang, Z., Hu, H., 2014. Auxetic materials and their potential applications in textiles. Text. Res. J. 84 (15), 1600–1611.

Yang, L., Harrysson, O., West, H., Cormier, D., 2015. Mechanical properties of 3d re-entrant honeycomb auxetic structures realized via additive manufacturing. Int. J. Solids Struct. 69–70, 475–490.

Yang, W., Li, Z.M., Shi, W., Xie, B.H., Yang, M.B., 2004. Review on auxetic materials. J. Mater. Sci. 39 (10), 3269–3279.

Yao, Y.T., Alderson, A., Alderson, K.L., 2008. Can nanotubes display auxetic behaviour? Phys. Stat. Solidi (b) 245 (11).

Zhu, H.X., Hobdell, J.R., Miller, W., Windle, A.H., 2001. Effects of cell irregularity on the elastic properties of 2d voronoi honeycombs. J. Mech. Phys. Solids 49 (4), 857–870.